Draft Technical Memorandum

Title: Ultra-High-Performance Concrete (UHPC) Use in Florida Structural Applications

FDOT Contract Number: BDV31 977-105

Task 1: Updated Literature Review Focusing on Fabrication, Inspection, and Testing of UHPC

Submitted to
The Florida Department of Transportation Research Center
605 Suwannee Street, MS 30 Tallahassee, FL 32399

c/o Dr. Harvey DeFord, Ph.D.
Steve Nolan, P.E.

Submitted by:

Dr. Kyle A. Riding (kyle.riding@essie.ufl.edu) (Principal Investigator)
Dr. Christopher C. Ferraro (Co Principal Investigator)
Dr. Trey Hamilton (Co Principal Investigator)
Dr. Joel Harley (Co Principal Investigator)
Raid S. Alrashidi
Megan Voss
Daniel Alabi
Engineering School of Sustainable Infrastructure and Environment
University of Florida
Gainesville, Florida 32611

January 2020

Department of Civil Engineering

Engineering School of Sustainable Infrastructure and Environment

College of Engineering

University of Florida

Gainesville, Florida 32611

Disclaimer

The opinions, findings, and conclusions expressed in this publication are those of the authors and not necessarily those of the State of Florida Department of Transportation or the U.S. Department of Transportation.

Prepared in cooperation with the State of Florida Department of Transportation and the U.S. Department of Transportation.

Approximate Conversions to SI Units (from FHWA)

Symbol	When You Know	Multiply By	To Find	Symbol
Length				
in	inches	25.4	millimeters	mm
ft	feet	0.305	meters	m
yd	yards	0.914	meters	m
mi	miles	1.61	kilometers	km
Area				
in^2	square inches	645.2	square millimeters	mm^2
ft^2	square feet	0.093	square meters	m^2
yd^2	square yard	0.836	square meters	m^2
mi^2	square miles	2.59	square kilometers	km^2
Volume				
fl oz	fluid ounces	29.57	milliliters	mL
gal	gallons	3.785	liters	L
ft^3	cubic feet	0.028	cubic meters	m^3
yd^3	cubic yards	0.765	cubic meters	m^3
NOTE: volumes greater than 1000 L shall be shown in m^3				
Mass				
oz	ounces	28.35	grams	g
lb	pounds	0.454	kilograms	kg
Temperature (exact degrees)				
°F	Fahrenheit	5 (F-32)/9 or (F-32)/1.8	Celsius	°C
Illumination				
fc	foot-candles	10.76	lux	lx
fl	foot-Lamberts	3.426	candela/m^2	cd/m^2
Force and Pressure or Stress				
lbf	pound-force	4.45	newtons	N
lbf/in^2	pound-force per square inch	6.89	kilopascals	kPa

Activities Performed During Period project start to 01/15/2020

TASK 1 – Updated Literature Review Focusing on Fabrication, Inspection, and Testing of UHPC

Status: This task is complete

1. Literature Review

1.1. Introduction

Ultra-high-performance concrete (UHPC) is a material with high compressive strength, high tensile strength, and ductility from the use of fibers. It has the potential to provide a very long service life for reinforced concrete structures, providing an alternative to polymer or stainless-steel reinforcement in extremely aggressive environments. The improved mechanical and durability characteristics of UHPC are due to its very dense microstructure and high volumes of well-distributed fibers that keep crack widths very small. The low porosity of UHPC is obtained by use of low water-cementitious materials ratios (w/cm) and high particle packing densities. Particle packing methods are used to optimize space filling and reduce the need for water to fill space and provide lubrication. Large quantities of different blends of cementitious materials and fine sands are used to optimize particle packing. Some of the properties that make UHPC such an excellent material for transportation infrastructure also necessitate in some cases different quality control test methods and field procedures to ensure that expected durability and mechanical property performance are achieved.

A review was made of UHPC construction methods to examine potential process requirements to achieve durable concrete and prevent material weakness from preferential fiber orientation or segregation. Durability, mechanical property test methods, and performance were also reviewed to identify candidate test methods and gaps in knowledge to help guide the experimental research program. A review of non-destructive methods that could be used to quantify fiber orientation and distribution of UHPC in structural members was also made.

1.2. UHPC Materials and Mixture Proportions

The formulation of non-proprietary UHPC mixtures requires particle size optimization through the use of several different cementitious materials and fine aggregates. Portland cements with a lower content of C_3A, sulfate, alkali content, and fineness are preferred because they have less negative impact on the workability and consequent entrapped air content [1]. Large quantities of supplementary cementitious materials are used, particularly silica fume and often slag cement. Silica flour can also be used [2]. A fine sand is used for the aggregates. Very high dosages of high-range water-reducing admixture are used, along with in some cases hydration stabilizers. Fibers are used to give the concrete a high tensile strength and in some cases give the UHPC strain-hardening properties. Steel is usually used between 1 and 4 percent by volume, however glass or PVA fibers are sometimes used for non-structural architectural panels [3]. Some examples of constituent material and mixture designs used for UHPC are presented in Table *1*.

Table 1: Typical material constituent and mixture designs for UHPC

Reference	Powder lb/yd3 (kg/m3)	Chemical admixture (SP) lb/yd^3 (kg/m^3)	Fine aggregate lb/yd^3 (kg/m^3)	Water lb/yd^3 (kg/m^3)	Fiber lb/yd^3 (kg/m^3)
FHWA[4]	1846 (1095) (Class H oil well CEM + SF)	24 (14)	1655 (982)	278 (165)	416 (247) (steel)
Meng et al.[5][6]	1807 (1072) (Type III CEM+FA+SF)	20 (12)	1704 (1011)	288 (171)	263 (156) (steel)
	1807 (1072) (Type III CEM+FA+SF)	22 (13)	1610 (955)	288 (171)	209 (124) (steel + synthetic)
	1896 (1125) (Type III+CEM+SL+SF)	22 (13)	1682 (998)	281 (167)	263 (156) (steel)
Wille et al.[7]	2048 (1215) (Type I CEM+SF+GP)	7 (4)	1761 (1045)	300 (178)	332 (197) (steel)
Park et al.[8]	1910 (1333) (Type I CEM+SF+GP)	98 (58)	1595 (946)	290 (172)	265 (157) (steel) (micro + macro)
Yu et al.[9]	1938 (1150) (Type I CEM +FA+SF)	56 (33)	1603 (951)	334 (198)	263 (156) (steel)
El-Tawil et al.[10]	1633 (969) (Type I CEM +SL+SF)	39 (24)	1971 (1169)	264 (157)	265 (157) (steel)
	1633 (969) (Type I CEM +SF)	17 (10)	2056 (1220)	278 (165)	

1.3. Fabrication Methods

Enhanced quality control is required to ensure members made with UHPC have the desired structural properties. Like normal-strength concrete, the quality of UHPC can be highly affected by the mixing and placement methods used. Because of the low w/cm and high fiber volume, UHPC requires more mixing energy than normal-strength concrete. UHPC is designed to be self-consolidating, but planning is needed to prevent fiber orientation and segregation problems, cold joints, and achieve an acceptable finish. UHPC curing will affect the hydration rate and type of product formed, greatly affecting strength, dimensional stability, and durability.

1.3.1. Mixing

Compared to conventional concrete, a higher energy is required during the mixing of UHPC. In order to obtain this amount of mixing energy, the mixing time is often increased. UHPC mixing time is often longer than 10 minutes. It can be reduced by carefully optimizing the mixture proportions, increasing the speed of the mixer, or using a high-shear mixer [11]. The UHPC mixing sequence is an important factor to ensure uniformity and consistency. Dry ingredients are usually added first to disperse ingredients and break down agglomerations by the shear action. The admixtures and water are then added, and the mixing is continued until fluidity is optimized. The fibers are sometimes added at the beginning if a high shear mixer is used. The actual mixing procedure may vary.

1.3.2. Placement method

The placement method may affect the mechanical properties of UHPC. The strength and tensile performances are highly influenced by the fiber orientation [12]. Fibers tend to orient themselves in the direction of concrete flow [12]. The degree of preferential orientation depends significantly on the placement methods, concrete viscosity, and flow distance [13]–[15]. Consequently, the placement process is a primary consideration when planning UHPC member fabrication.

The rheological properties of UHPC are affected by the content, material, and type of fibers. As the fiber content increases, the viscosity and yield stress increase leading to a decrease in workability and an increase in the probability of fiber interlock. When the fiber content exceeds a critical fiber concentration, the fibers can form clumps and balls, which make it hard for placement operations. Fiber balls can also result from locally high fiber concentrations from poor mixing

[16]. Fiber agglomeration usually results in an unworkable mix; therefore, as UHPC mixes tend to stiffen rapidly, the placement should be done quickly. Internal vibrators are not allowed for UHPC because they can cause preferential orientation or even sedimentation of the fibers. Limited external vibration could be used for 1 or 2 seconds to facilitate release of entrapped air [17], [18].

Placement techniques can influence the amount of preferential fiber orientation. While there is a concern that preferential orientation could cause weak zones or directions, preferential orientation of fibers can be used to increase the UHPC tensile strength where desired and increase the efficiency of the fibers [13], [19], [20]. Crack bridging by preferentially-oriented fibers reduces the widths of transverse cracks and increases the composite tensile strength in the direction of orientation. Strengths perpendicular to the direction of orientation are lower due to the reduced number of fibers oriented primarily in the transverse direction. The effect of concrete placement speed on fiber orientation was evaluated by moving a chute at 5 in./s, 10 in./s and 20 in./s. Wille and Parra-Montesinos [11] found that increased speeds created thin ribbon-like layers in the UHPC that would give a preferred fiber orientation along the length of the beam and better flexural strength results in beams tested according to ASTM C1609 samples [10]. Another study looked at two placement methods: a direct method, and use of an L-shaped device to control the flow of UHPC and provide fiber orientation [23]. The results of flexural strength, toughness, and modulus of rupture were compared. The UHPC specimens prepared by the L-shape device exhibited higher mechanical properties, 64.3%, 65.1%, and 77.1%, respectively, compared with specimens prepared by a direct-cast method. The effect of two different placement methods, placing the concrete at the center and the corner of the UHPC specimen, on the ultimate flexural strength was investigated (Yoo et al., 2014). The specimens with concrete placed in the center showed higher flexural strength because of better fiber dispersion with more fibers at the crack plane [24]. Another study examined the effects of fiber orientation on reinforcing bar pullout strength and used a casting device (chute) with sixteen channels to control the flow of UHPC [25]. The measurements were taken using pullout specimens with perpendicular, parallel, and random fiber orientation. The results showed that the specimens with fibers orientated perpendicular to the load direction recorded the highest pullout forces, followed by the random orientation, and then the parallel orientation [25].

While studies have shown that fibers can be preferentially oriented on purpose, planning is critical to prevent problems. Concentrating the fibers in one direction requires that the member will have a lower percentage in other directions, giving lower tensile strength in that direction. Most studies on concrete fiber orientation control have been conducted on small specimens or slabs. For long-line prestressed members, work is needed to determine how to prevent fibers from preferentially orienting in the direction of the prestressing.

1.3.3. Curing methods

Curing methods greatly affect UHPC microstructural development, which has a large impact on mechanical and durability properties. The most popular methods of curing to provide a necessary environment for the concrete are water curing, hot air curing, steam curing, and autoclave curing. In addition to accelerating cementitious material hydration, higher curing temperatures are used to change the type and microstructure of hydrates formed.

In UHPC, there is a strong relationship between curing temperature and the development of strength. For a precast UHPC plant, standard steam curing can be used to ensure rapid strength development. For one UHPC pedestrian bridge tested, the early strength was reduced from 215 to 147 MPa when the 194°F (90°C) steam curing was lowered to 158°F (70°C) [26]. Koh et al. showed that while concrete cured at ambient temperatures can attain a 90-day strength similar to that of steam-cured concrete, the strength during the first week is significantly lower [27]. Florida precast concrete producers, however, do not like to use steam because of the cost. The high ambient temperatures in Florida, the use of insulation, and the high heat of hydration of UHPC mixtures can still lead to high in-place temperatures and rapid strength gain without added heat. Yazici investigated the effect of curing condition on the mechanical properties of UHPC and concluded that steam curing seemed to be effective for increasing the compressive strength; however, it caused a reduction in flexural strength compared to standard curing at 28 days. This was thought to be because of the decreased bond strength between matrix and fibers [28].

Arunachalam and Vigneshwari found that oven-curing increased UHPC compressive strength [29]. However, in a study done Gu et al., it was observed that oven curing led to lower chloride and freeze-thaw resistance when compared to standard and steam curing. This thought to be because of internal micro-cracks that formed [30]. When oven curing is used, the coupled effects of both mechanical and environmental loads will play a role in determining the durability of UHPC structures [30]. More work is needed to examine the impact of curing temperatures on concrete durability properties.

The particular phases that form under ambient and elevated temperature curing will depend on the particular composition of UHPC used. Curing UHPC under lab temperature gives similar types of hydration products as normal-strength concrete. This includes calcium-silicate-hydrate (C-S-H), calcium hydroxide (CH), alumina, ferric oxide, monosulfate phases (AFm) and alumina, ferric oxide, trisulfate (AFt) phases. Differences in the quantities of hydration products will occur because of the pozzolanic reactions from high amounts of SCMs. The pozzolanic reaction that happens when silica fume reacts with calcium hydroxide to form calcium silicate hydrate (C-S-H) is activated under high temperature [31], [32]. C-S-H has been found to stay amorphous up to at least 194°F (90°C) [31].

Microstructural studies of autoclaved UHPC have found that phases, hydration product crystallinity, and porosity change as the temperature increases above 212°F (100°C) and the pressure increases. One study found that porosity reached a minimum when the concrete was cured between 302° and 392°F (150° and 200°C). When there are pozzolans to provide silica to react with calcium hydroxide, the Si/Ca ratio in crystalline calcium-silicate-hydrate phases formed also increases [33]. Heat treatment leads to phases such as foshagite, xonotlite, and jaffeite with portlandite still present. Autoclaving leads to the disappearance of portlandite. Afwillite, foshagite, and xonotlite can form at pressure above 72.5 psi (5 bars) temperatures above 302°F (150°C). Afwillite, foshagite, tobermorite, and xonotlite can form at pressures of 218 psi (15 bars) and temperatures above 392°F (200°C) [33]. Crystalline calcium-silicate-hydrate fill in porosity that normally would be empty, giving much higher compressive strength for UHPC when autoclaved [33]. Calcium hydroxide content is significantly reduced from pozzolanic reactions under autoclave conditions. The bound water content of hydrates also changes, altering hydration product density and space-filling ability [34].

1.4. Fresh Concrete Properties

The low water-cementitious material ratio, high paste content, and use of high volumes of fibers impart different fresh properties on UHPC than are typical for normal-strength concrete. A review of the causes of these properties and test methods used is provided.

1.4.1. Use of chemical admixtures

The superior mechanical and durability of UHPC is due mainly to the use of very low water-cementitious material ratios (w/cm). The low water mixture content of UHPC can give the mixture poor workability; therefore, high dosages of high-range water-reducing admixtures or superplasticizers are needed to achieve its fluidity. In order to understand concrete fresh properties, a discussion of the role of superplasticizers is helpful. Superplasticizers are used to reduce the concrete yield stress. Most superplasticizers do very little to the concrete viscosity, resulting in very sticky mixtures [35]. Superplasticizers improve the workability of concrete by adsorbing onto cement particles and providing electrostatic repulsion and steric hindrance to reduce particle flocculation [36]. Different types and dosages of superplasticizer will show different effects on the fresh and hardened properties of UHPC. Plank et al. [26] used two different types of superplasticizers, methacrylic-acid-ester-based and allyl-ether-based, in UHPC mixes having cement and silica fume. They reported that methacrylic-acid-ester-based superplasticizers interacted well with cement but not with silica fume, and the allyl-ether-based superplasticizers were more effective with silica fume. Using both of them resulted in better dispersion and interaction [37]. The incorporation of chemical admixtures is known to affect the total porosity and the pore size distribution [38]. Insufficient dosages of superplasticizers would make the fluidity of UHPC low and lead to a higher percentage of porosity. Courtial et al. studied the effect of different dosages of polycarboxylates on the microstructure of UHPC. They found that when the addition of polycarboxylate was modified from 1.8% to 2%, the belite phase content significantly decreased [39]. Wille et al. studied 38 UHPC mixtures and concluded that based on the best spread value of the paste and entrapped air content, the optimum amount of superplasticizer (polycarboxylate ether-based) ranged from 1.4% to 2.4% of cement by weight [40].

It was reported that the workability of concrete is usually controlled by the density of the side chain of superplasticizers, whereas the retardation time is mainly influenced by the length of the side chain [41]. Hirschi et al, investigated eight types of polycarboxylate-based superplasticizers on the setting time and strength of UHPC [42]. The setting time had some variation but showed a good indication for the development of early compressive strength [42]. Mixtures having superplasticizers with long side-chain length showed the highest early strength compared to those which had medium side length [42]. Clearly, superplasticizer selection and dosage will greatly impact UHPC flow and setting properties.

1.4.2. Rheology

Compared to conventional concrete, UHPC has a higher viscosity. This is owed to the very low w/cm and use of large dosages of superplasticizers that often do little to lower the viscosity. Therefore, its rheological properties should be assessed during trial batches and structural member mockups to ensure it can be placed. Rheological evaluation of the cement paste helps in understanding the flow characteristics and the development of the early-age structure in pastes. The flow and pumping performance can be evaluated by rheological behavior as well [43]. Many test methods have been used to evaluate the yield stress and/or plastic viscosity of UHPC, such as mini-slump, mini V-funnel flow test, modified slump test, portable vane test, and inclined plane test [16]. However, among these test methods, the mini-slump test is the easiest way to characterize the flowability of the fresh paste of UHPC as it is inversely related to yield stress.

The flow test is typically used to measure the placeability of mortar in its fresh state. Since UHPC does not typically use coarse aggregates, the flow test with some modifications has become a widely used test for fresh UHPC. When used with UHPC, it is usually referred to as the mini-slump test and can be performed in the field for quality control testing. ASTM C1856 "Standard Practice for Fabricating and Testing Specimens of Ultra-High Performance Concrete [44]" modifies ASTM C1437 "Standard Test Method for Flow of Hydraulic Cement Mortar [45]" for UHPC to account for its unique properties. ASTM C1856 does not allow tamping in the mold or table-dropping to aid flow because UHPC is designed to be self-consolidating. This allows for the flow table to be taken off of the concrete pedestal normally used, making it field-portable, as shown in Figure 1. The brass cone mold is filled with UHPC in a single layer without tamping, as shown in Figure 2. The excess concrete is screeded using a small rubber bar [46]. Once filled and screeded, the cone is lifted to allow UHPC to spread evenly on the table. Spread measurements are taken after 120 ± 5 s to allow the self-consolidating UHPC time to stop flowing [46]. A flow between 8 and 14 in. (203 and 366 mm) is typically recommended to ensure concrete flowability [17]. Figure 3 shows UHPC at the end of a flow test with measurement of 8.5 inches (216 mm).

Figure 1: Flow table at the field

Figure 2: Filling the mold with UHPC

Figure 3: Static flow test with measurement of 8.5 in.

A method to calculate concrete fundamental rheological properties from the mini-slump test has been developed. Roussel et al. proposed a theoretical approach to estimate the yield stress of the cement paste from the mini-slump test by using a viscometer. Their approach used the final spread diameter of the mini-slump test, the surface tension of the fluid, and the contact angle between the fluid and the test surface to model the rheological properties [47]. A study done by Tregger et al. made different mixtures to measure the viscosity and yield stress by using a rheometer, plus the mini-slump test was performed simultaneously [48]. They confirmed good correlations between the yield stress and mini-slump flow and between the final spread time and viscosity/yield stress ratio [48]. Choi et al. proposed a more accurate method by considering the changes in final diameter according to the time measured at the mini-slump test [49]. A computational fluid dynamic analysis was used to simulate the mini-slump test and compared it to mini-slump experiments on four different UHPC mixtures. It was concluded that by applying the mini-slump test, the UHPC rheological properties could be easily estimated [49].

The very low water-cementitious ratio (w/cm) of UHPC can cause problems with slump loss due to evaporation leading to a big impact on the consistency of the mix. Therefore, many U.S. states require UHPC to be placed continuously and monolithically to avoid problems at the interface between placements as well as cold joint problems that may occur from the formation of elephant skin [50], [51]. Cold joints may occur when having two placements of UHPC as elephant skin forms quickly on the surface of UHPC and hinders bonding of the layers as shown in Figure 4. Cold joints as a result of delays during concretes placement may occur quickly and randomly in unexpected locations and can lead to cracking. Lee et al. studied the effect of placement delays up to 60 minutes on the bonding shear performance. The results showed that a good bond could be developed if the delay was kept to 15 minutes or less, with only an 8% reduction in shear strength expected. After 15 minutes, however, a large drop in the bond strength was found [52]. It is recommended that a form liner or mesh be used to create a fluted surface to increase interlock and bond strength between adjacent placements of concrete. [53]

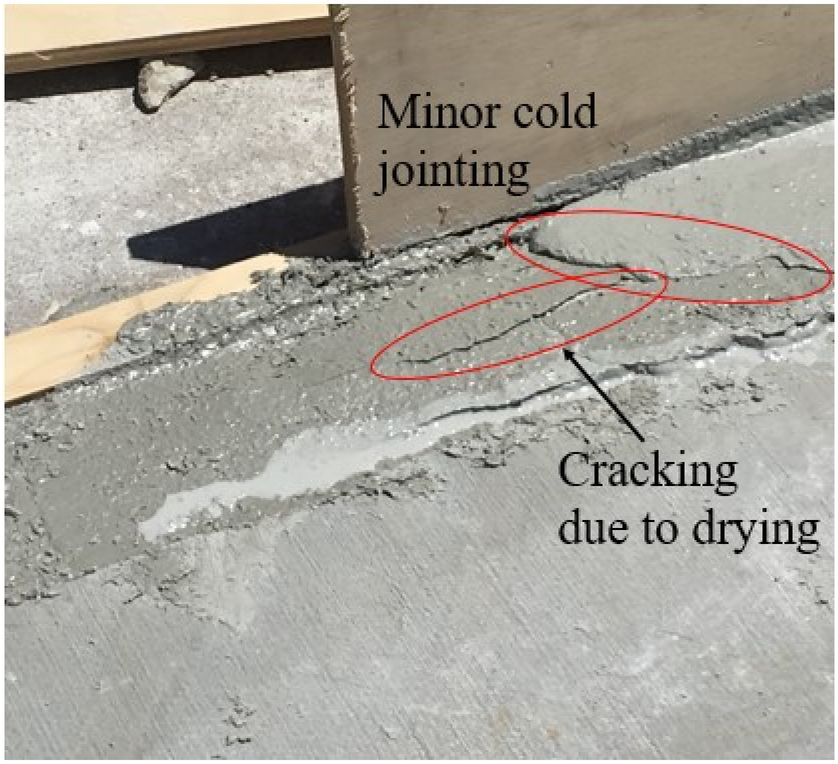

Figure 4: Defects in a UHPC joint due to placement procedure

1.4.3. Setting time

UHPC will often have longer initial and final setting times than normal concrete because of the large quantities of high-range water-reducer used. UHPC initial and final time of set is usually measured by penetration standard method ASTM C403 “Standard Test Method for Time of Setting of Concrete Mixtures by Penetration Resistance [54]” or by Vicat Needle method ASTM C191 “Standard Test Methods for Time of Setting of Hydraulic Cement by Vicat Needle [55]” with some alterations mentioned by ASTM C1856. In the ASTM C403 standard method, a penetration needle is pressed into mortar in a rigid container with dimensions at least 6 in. (152 mm) in width and 6 in. (152 mm) in height. The penetration needle is attached to a press with a load cell or other device to measure the force and with a dial gauge to record the penetration distance into the concrete. The maximum force when the needle penetrates at least 1 in. (25 mm) into the UHPC sample is recorded periodically [54]. The time when the pressure required to insert the needle 1 in. (25 mm) reaches 500 psi is considered the time of initial set and the time when it reaches 4000 psi is considered the time of final set.

ASTM C1856 modifies ASTM C191 for use on UHPC with only minor changes. In this test, UHPC instead of cement paste is placed into a conical ring without consolidation. The sample is made to the specified flowability for the project instead of a normal consistency as is typically used. A 0.039-inch (1-mm) diameter needle with a 0.66 lb (300 ± 0.5 g) weight attached on top is dropped onto the sample inside a conical ring. The test is repeated periodically on different spots on the sample. In between tests, the sample is stored in a moist room, limiting applicability of this test to laboratory use and material prequalification. The initial setting time is taken as the elapsed time between mixing and when the weighted needle penetrates 1 in. (25 mm) into the surface. When no penetration is observed, the elapsed time from molding to that point is the Vicat final setting time [55].

To illustrate the effect that high admixture doses can have on the concrete time of set, some cases in the literature are highlighted. In one study, four different UHPC mixtures were tested using the penetration resistance test. The initial setting times ranged from 70 minutes to 15 hours, and final setting times were between 5 hours and 20 hours [17]. In some UHPC mixes, based on the type and dosage of chemical admixtures, the UHPC can have an initial set time as low as 90 minutes and final setting time of 7 hours [56]. The difference in setting time can be attributed to differences in superplasticizer type and dosage, and in some cases the use of accelerators.

Due to the thixotropic properties and low w/cm of some UHPC mixes, the initial and final set times can be difficult to measure accurately. In one study, Graybeal tested the setting times of six different UHPC mixes and reported that one of them could not be measured due to the needle not being able to penetrate the sample. If left undisturbed, UHPC can form a strong surface layer called an elephant skin that can inhibit needle penetration. The rest of the mixtures tested had initial set times ranging from 4.3 hours to 9 hours and final set times from 7 hours to 24 hours [4].

1.5. Mechanical Properties

UHPC has high compressive strength; however, without fibers it has very brittle behavior. Fibers between 1 and 4% are commonly used to increase its ductility, with many mixtures exhibiting strain-hardening characteristics. If the UHPC tensile toughness can be provided reliably in concrete structural members, this could lead to a reduction in mild steel reinforcement requirements.

Testing is needed to verify concrete tensile properties to assure good structural performance. Several test methods have been proposed for quantifying the concrete tensile properties. These tests can be classified as flexural, panel, splitting, compact tension, or direct tension tests. Each type of test has its advantages and drawbacks. Variations of each type of test have been developed for plain or fiber-reinforced concrete to try to solve some of these issues for specific purposes. Instead of reviewing the dozens of variations of these tests in detail, this review will focus on tests that have been suggested for quality control testing, and that show the greatest promise. Consequently, panel tests will not be considered because of the size sample required and difficulty for labs to routinely test. Although compact tension tests can provide important fracture toughness information, they are difficult to run, require specialized equipment, and have a high coefficient of variation, so they will not be described in detail in this report [57].

1.5.1. Flexural tests

Several flexural tests have been developed to indirectly measure concrete tensile properties. These tests attempt to measure the concrete deflection or crack opening under load as a measure of the concrete ductility and toughness. They are typically based on three- or four-point bending tests, with some beams made with notches [58]. This review will focus on two that have a history of use in the United States and have the most potential for adoption as a quality control test if modified.

ASTM C1018 "Standard Test Method for Flexural Toughness and First-Crack Strength of Fiber-Reinforced Concrete (Using Beam with Third-Point Loading)" [59] measures the concrete beam middle deflection when placed under third-point loading. The tensile stress-strain response of UHPC can be divided into four sequential phases: elastic behavior, brittle behavior - formation of many cracks in the UHPC matrix that are perpendicular to the direction of applied stress, crack straining where the individual cracks widen, and the localization stage where the individual cracks reach the strain limit [11]. The concrete toughness is defined as the area under the load-deformation curve up until a specified beam deflection [59]. This test was discontinued in 2006 and has only been used sparingly for UHPC. One study found a small difference in performance when steam curing was used. The modulus of rupture values for the first cracks were 1.3 ksi for the untreated specimens and between 1.3 ksi to 1.5 ksi for steam-cured specimens [11].

ASTM 1609 "Standard Test Method for Flexural Performance of Fiber-Reinforced Concrete (Using Beam with Third-Point Loading)" [21] has become a common method to use for measuring the flexural performance of UHPC. In this method, a simply supported beam is tested under third-point loading as shown in Figure 5. An example of a specimen in the test machine is shown in Figure 6. The size of the UHPC specimen tested is based on the maximum fiber length. Longer fiber lengths require larger cross-sections [46]. The deflection of the sample middle compared to the supports is measured by securing a jig onto the sample above the supports and measuring the distance between a bar connecting the two points above the supports to the top of the sample middle. The sample is loaded using deflection control and not displacement or force control. The loading rate is kept between 0.002 to 0.004 in./min until a net deflection of L/900 of a specimen is reached. Assuming linear-elastic response up until the first-crack occurrence, the first peak deflection can be estimated using Equation 1:

$$\delta_1 = \frac{23P_1L^3}{1296EI}\left[1 + \frac{216d^2(1+\nu)}{115L^2}\right] \qquad \text{Equation 1}$$

Where: δ_1 is the first peak deflection in inches
P_1 is the first peak load in lbf
L is the total beam span length in inches.
E is the estimated modulus of elasticity in psi.
I is the cross-sectional moment of inertia in inches
d is the average depth of the specimen at fracture in inches
ν is Poisson's ratio

After a deflection of L/900 is reached, the loading rate can be increased between 0.002 and 0.008 in./min until reaching a net deflection of L/150 [21]. The residual first-peak strength values can be used to calculate the strength of the concrete by using Equation 2:

$$f = \frac{PL}{bd^2} \qquad \text{Equation 2}$$

Where: f is the residual first-peak strength, psi
P is the first-peak load, lbf
L is the span length, in.

d is the depth of the specimen at the point of failure, in.
b is the average width of the specimen at point of failure, in.

Using the first-peak strength, the equivalent flexural strength-to-toughness of the material can be determined from Equation 3:

$$R_{T,150}^{D} = \frac{150T_{150}^{D}}{f_1 bd^2} \times 100\% \qquad \text{Equation 3}$$

Where: $R_{T,150}^{D}$ is the equivalent flexural strength
T_{150}^{D} is the area under the load vs. net deflection curve 0 to L/150, J

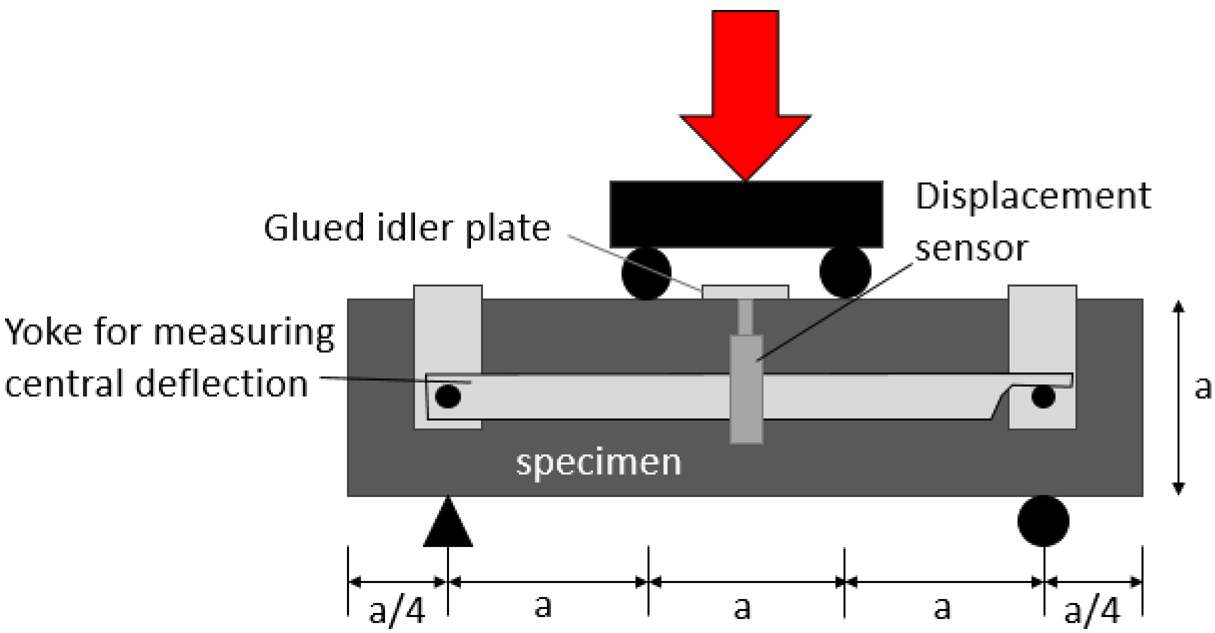

Figure 5: ASTM C1609 test schematic

Figure 6: Sample at University of Florida during testing according to ASTM C1609

ASTM C1609 may need some modifications in order to be used for quality control because many laboratories lack the ability to use deflection control to control the loading rate. Modifications may be possible to change the loading rate control method and deflection measurement method to simplify the test and widen the base of labs that could use it.

When loaded in flexure, the concrete beam section will have some regions in compression and some in tension. While the strain distribution with depth for the beam section may be linear, the stress distribution will not be because the UHPC tensile stress-strain relationship is not linear until failure. Inverse calculations are required to obtain the tensile stress-strain relationship. This requires either direct measurement of the concrete bottom strain, or assumption of the shape of the stress-strain curve [60], [61]. Assuming the shape of the stress-strain curve can result in non-conservative values [60]. Flexural tests have been shown to have a high coefficient of variation of up to 20% for fiber-reinforced concrete [58]. This is might be because of the span length-to-depth ratio may not be high enough.

1.5.2. Splitting tensile strength test

ASTM C496 “Standard Test Method for Splitting Tensile Strength of Cylindrical Concrete Specimens [62]” is commonly used to assess the tensile strength of concrete indirectly. In this test method, a cylinder is placed in a loading machine tested under a compressive load of 100 to 200 psi/min that is applied continuously along its side. The compressive force causes a split of the cylinder into halves. The tensile strength then can be calculated using Equation 4:

$$T = 2P/\pi l d \qquad \text{Equation 4}$$

Where: T is the ultimate splitting tensile strength (psi)
P is the ultimate load (lbf)
l is the specimen length (in.)
d is the specimen dimeter (in.)

This test is generally applicable for concrete, and since it includes assumption of mechanical behaviors that are not likely to be consistent with strain hardening fiber reinforced concrete, it needs to be modified to be applicable for UHPC. Graybeal proposed some modifications to ASTM C496 to allow it to be used with UHPC. These modifications include increasing the loading rate from 150 to 500 psi/min (1 to 3.5 MPa/min) due to the higher tensile strength of UHPC [63]. Also, since the initial cracking of UHPC occurs much earlier than the maximum tensile strength, the modified version includes using LVDTs across the middle of the cylinder, and spring-loaded clamps fitted onto the outside of the cylinder to transfer the transverse deformations to the transducers as shown in Figure 7 [63]. This allows for capturing the tensile cracking and post-cracking behavior electronically, thus calculating the tensile strength and ductility [63]. A downside of this test is it tends to inflate the tensile capacity of UHPC specimens due to differences in fiber pull-out behavior. Since cylinders are loaded in compression, it increases the normal force and friction on fibers preventing pull-out. Therefore, under this bi-axial stress state the fibers are able to hold a greater load before pulling out of concrete [63]. In fact, the discrepancy between splitting tensile strength and direct tension strength was shown to increase from 39% for plain concrete to 77% for UHPC with 3% by volume of steel fibers [64]. These discrepancies prevented widespread adoption of this test method.

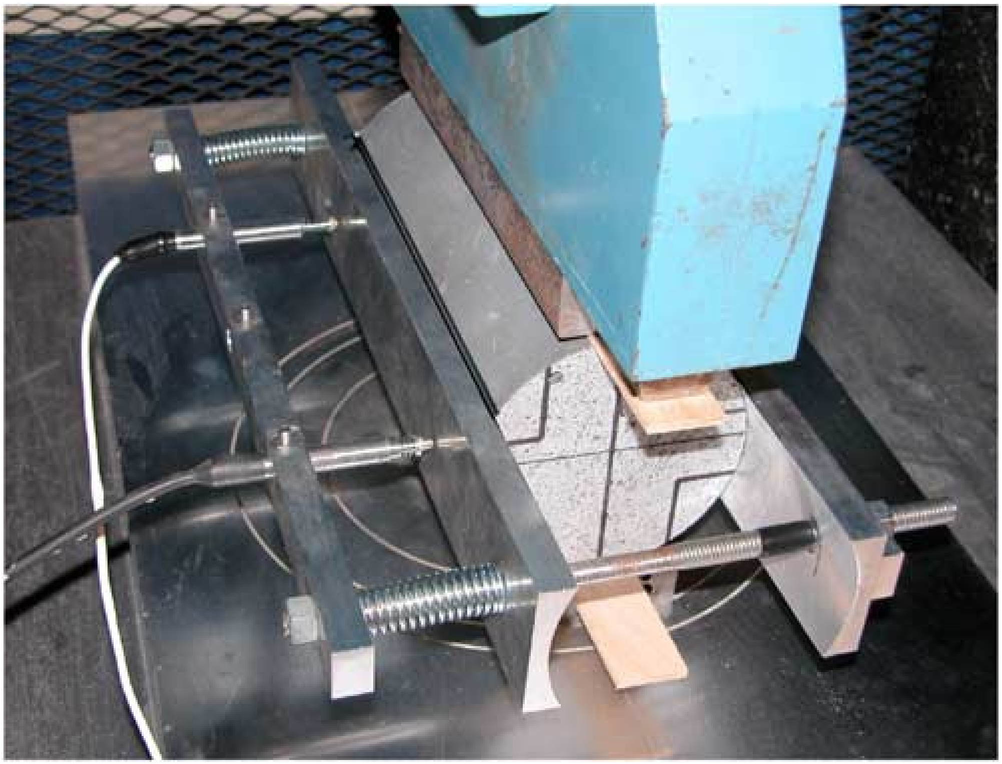

Figure 7: Splitting tensile test set-up (B. A. Graybeal, 2006b)

Compared to conventional concrete, UHPC splitting tensile strength is much higher. A study was done by Ozyildirim by testing UHPC beams for splitting tensile (Ozyildirim, 2011). The average splitting tensile strength was measured after the initiation of the first crack, which is considered to be the discontinuity in the load-displacement curve [63]. The results showed an average value of 1.47 ksi of splitting tensile strength with a standard deviation of 0.37 ksi, and an average apparent ultimate strength of 3.21 ksi with a standard deviation of 0.27 ksi (Ozyildirim, 2011). Haber et al. made 20 UHPC mixtures to be tested for splitting tensile. All these mixes exhibited approximately the same initial cracking strength of 1.0 ksi [4]. Another study on 15 UHPC mixes showed an average of 1.08 ksi for the initial cracking strength [60].

1.5.3. Double-edge wedge-splitting test

A double-edge wedge splitting test has been developed to force the center of a sample to undergo tension perpendicular to the direction of a load application. While different dimensions have been used on samples for this test [14], [57], [66], the concept is the same. Figure 8 shows a schematic of the sample cross section used in the test, which is typically square [57], [66]. A roller is used on the top and bottom notches to apply a normal force on each side of the notch. It can be run with and without the sawcut below the angled notch. This creates a tensile force perpendicular to the vector connecting the notches. The splitting force F_{sp} can be calculated using Equation 5 [66]:

$$F_{sp} = \frac{P \cdot (\cos\theta - f\sin\theta)}{2 \cdot (\sin\theta + f\cos\theta)} \qquad \text{Equation 5}$$

Where: P is the load (lb)
θ is the notch angle (°)
f is the friction coefficient of the roller-concrete interface

The displacement is monitored using linear variable differential transformers (LVDTs) placed near the tip of the top notch, in the middle, and near the tip of the bottom notch as shown in Figure 8. These displacements are used to get the crack opening displacements (COD) and rotations along any axes [66]. The test can be run using displacement control at a rate of 0.051 in./s until 0.078 in. of displacement is reached, after which the loading rate is doubled until 0.157 in. of displacement is reached. At that point, the displacement rate is doubled again until the test is complete and the specimen is split in half [57].

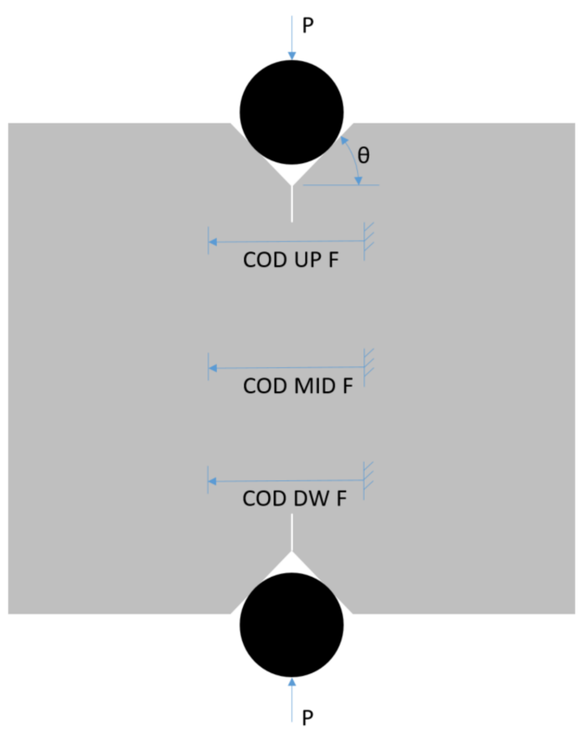

Figure 8: Schematic of double-edge wedge-splitting test [66]

This test is designed to avoid some of the drawbacks of the splitting tensile test. In the splitting tensile test, the concrete in the center of the sample will have compression in the vertical direction and tension in the horizontal direction, giving a biaxial state of stress. The compression force can add friction to fibers during pullout, changing their mode of failure. If friction can be eliminated between the concrete and the roller, this test can avoid that problem by placing forces at an angle and separated at the notch to eliminate the compression force in the concrete at the center [66]. This test method has a coefficient of variation of 14% [57].

While this test method could provide good information about the tensile stress-strain behavior of UHPC, implementation at precast plants and local testing labs would be difficult. It requires significant instrumentation to measure the displacement at three locations using LVDTs. The displacement rates required for this test would likely be difficult to control in a simple compression machine. Finally, the sample geometry is unconventional and would require new molds or time-consuming sawcutting.

1.5.4. Double-punch test

The double-punch test, also known as the Barcelona test, is a relatively simple test used to find tensile properties of fiber-reinforced concrete. It has been standardized as UNE 83515 in Spain [67], but is otherwise used mainly for research purposes. This specification is based on the original double-punch method developed over 50 years ago [68]. This original double-punch test was used to calculate a single tensile strength value of normal concrete. It was meant to be a replacement for the split-cylinder test, which is comparatively difficult to set up [68]. This test can be run with a cylinder with a 6-in. diameter and 6-in. height or with a 6-in. cube. A punch with a 1.5-inch diameter and 1-inch height is placed at the center of the specimen on both the top and bottom, as shown in Figure 9.

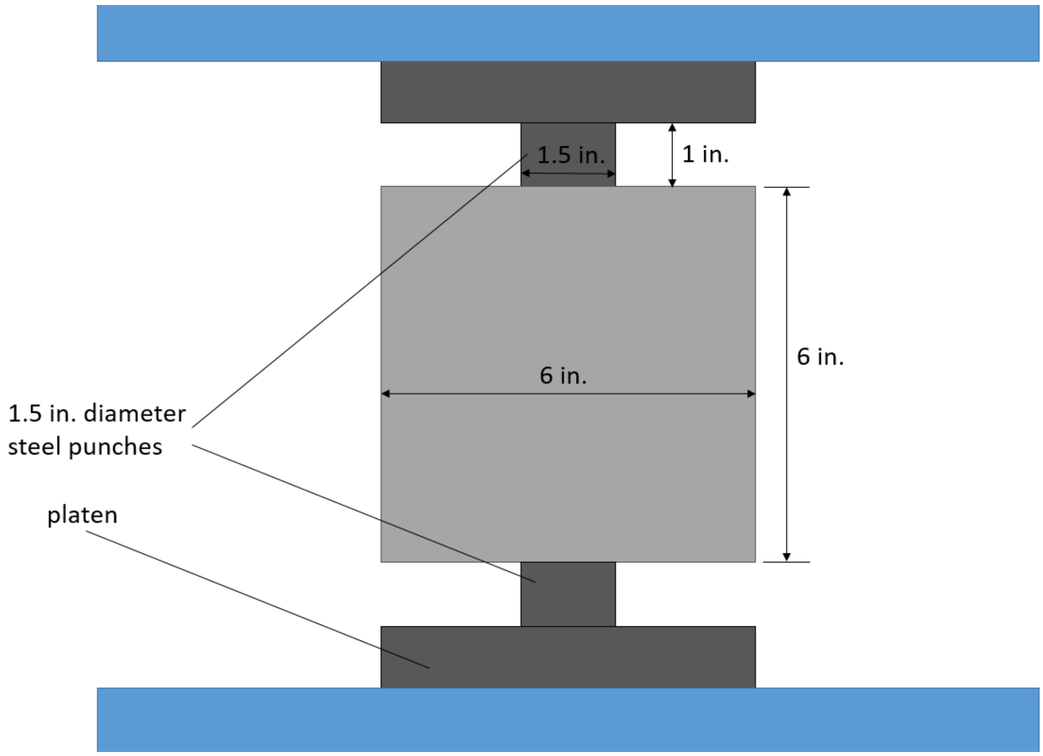

Figure 9: Double-punch test setup

The tensile strength from this test can be computed using Equation 6 as proposed by Chen (1973). It should be noted that in his 1969 paper, Chen uses a constant of 1.30 instead of 1.20 in the denominator [68].

$$f'_t = \frac{Q}{\pi(1.20 * bH - a^2)} \qquad \text{Equation 6}$$

Where:

f'_t is the tensile stress (psi)
Q is the applied load (lb)
b is the radius of the cylinder (in.)
H is the height of the cylinder (in.)
A is the radius of the punch (in.)

Chen stated that this equation is valid when either *b/a* or *H/2a* is less than or equal to 5 [68]. The ASTM draft ballot for standardization of the double-punch test adds a safety factor of 0.75 multiplied in the numerator of Equation 6 to convert load to stress [69].

At the end of testing, the specimen will usually have 3-4 cracks propagating from the edge of the punch outward. Figure 10 shows a schematic of a typical specimen after failure.

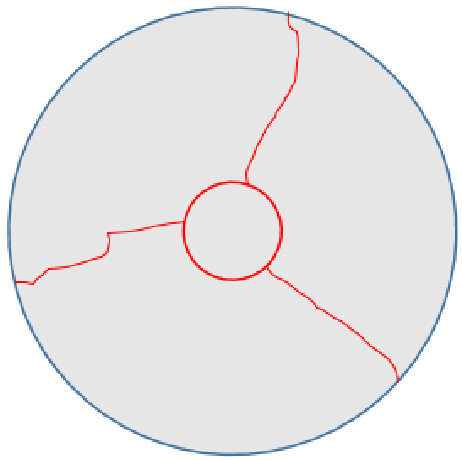

Figure 10: Typical double-punch failure

In order to modify this test method for fiber-reinforced concrete, crosshead displacement measurements were added. If a cylindrical specimen is used, the total circumferential opening displacement (TCOD) can be measured with a chain extensometer [70]–[72]. A typical load vs. displacement relationship is shown in Figure 11. This gives a curve of load vs. TCOD. Due to the cost and complexity associated with measuring the TCOD, some researchers have measured the axial displacement instead [70]–[72]. This can be done by measuring the distance between the top and bottom surfaces on the machine or by using the crosshead displacement output on the machine used for testing. A typical result of this method is shown in Figure 12 [70]–[72]. As shown in this figure, there is an extended period of displacement without load in the beginning of the load vs. axial displacement graph. This region occurs when there is local crushing at the punch location, but full cracks have not yet formed in the specimen. When axial displacement is plotted vs. TCOD, a result similar to that depicted in Figure 13 is formed [70]–[72].

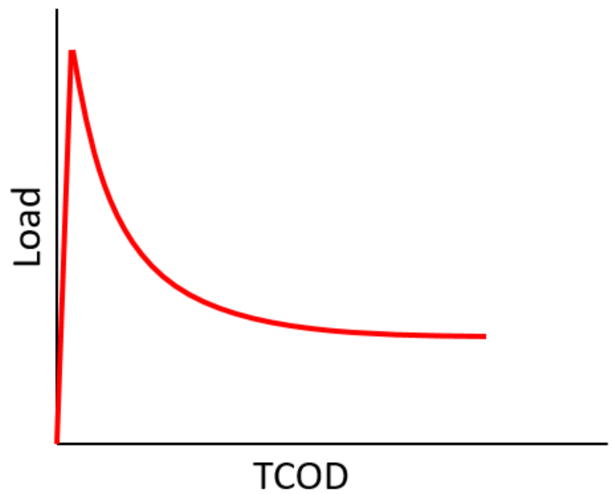

Figure 11: Typical load vs. circumferential displacement curve

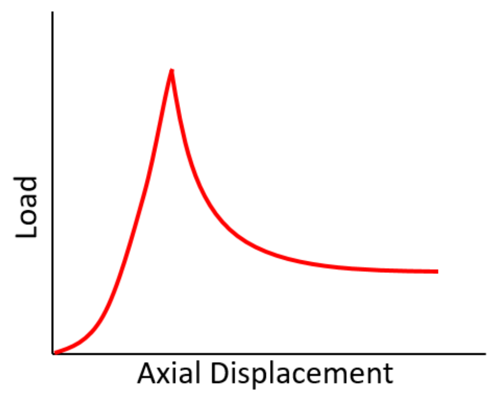

Figure 12: Typical load vs. axial displacement curve

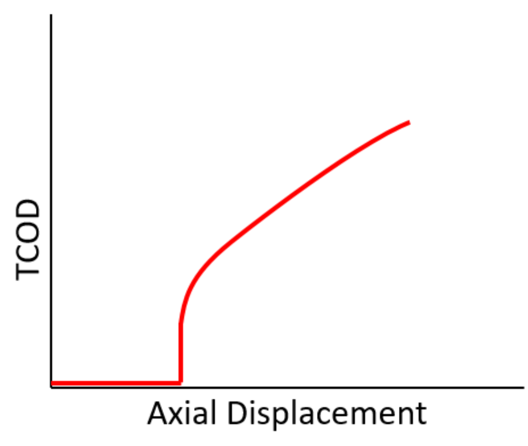

Figure 13: Typical circumferential displacement vs. axial displacement curve

From the load vs. displacement data, multiple characteristics can be determined. In addition to the peak strength, as originally used by Chen [68], users of this test can also determine ductility of the sample. This can be done in multiple ways. First, the user could find the strength at a particular displacement past where the peak load occurs. Or, the user could find the displacement at which the strength drops below a particular load value. The residual strength (strength of fiber bridging after cracking) can also be found [72]. This value would occur after the concrete cracks and the load declines, beginning to level out. While defining the exact value of residual strength may be difficult due to the sloping load curve [72], it can be useful for comparison as it would increase with a higher dosage of fibers or better fiber pullout strength. This test can also be used to measure toughness [72], which is especially of interest for impact resistance.

The overestimate of tensile strength measured by the double punch test over that measured by direct tension testing has been shown to decrease with increasing fiber content, from 11% with plain concrete to 4% with 3% steel fibers [64]. The double punch test has also been shown to have a low coefficient of variation of between 9 [58] and 12% [73].

1.5.5. Direct tension test

Direct tension test methods can more realistically predict the tensile strength and ductility behavior than indirect test methods. Many different test methods have been proposed to test direct tension with different geometries (for example, notched and unnotched prism or cylinders, dog-bone or dumbbell shape) and various types of gripping or attachment systems (e.g. fixed or rotating boundary condition) [74]. More than 25 different configurations have been identified for UHPC direct tension testing [74], [75]. There is no standard method however for direct tension testing of UHPC.

After several iterations of improvement, the Federal Highway Administration (FHWA) has recommended a direct tension test method for UHPC [60], [75]. The test method uses a dog-bone shaped specimen with a dimension of 2 × 2 × 17 in. Aluminum plates are epoxied to each side on both ends as shown in Figure 14. Hydraulic grips of the universal testing machine are used to grip the samples and apply the tensile force to the specimens. The aluminum plates are added to the sample ends to reduce the crushing of the specimens during gripping and strengthen the sample where gripping forces and stress concentrations occur. This helps ensure that the cracks and sample failure occur in the sample center where the strain is measured. Some modifications were proposed to help prevent test failure around the end of the plates. These modifications were to use a small compressive force in the tapered portion of the aluminum plates and to use some clamps to prevent the plates from delaminating during loading as shown in Figure 15 [50].

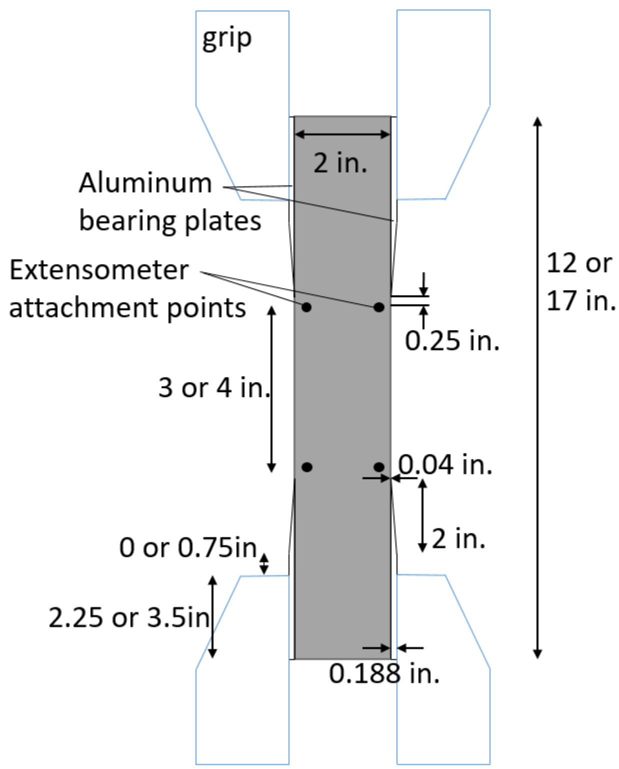

Figure 14: Schematic of direct tension UHPC test specimen

Figure 15: Tensile test before gripping with the C-clamps attached

While direct tension tests provide important information needed for structural design obtained during the material prequalification, none of the direct tension tests developed to date show promise for use in project quality control operations. The direct tension test proposed by FHWA [60] and that recommended by Riding et al. [50] are too complicated for use by precast plants and local testing labs and require expensive equipment, limiting their utility to qualification testing. Direct tension test methods possibilities that are simple such as briquette tests have been found to be too variable, difficult to get the sample aligned and avoid bending [50], or subject to fiber alignment issues [74].

1.5.6. Compressive strength

The compressive strengths of mortar and concrete are typically used as an initial indication of their quality. UHPC strengths have been reported to exceed 150 MPa and are governed by many factors such as curing method, fiber shape and content, and testing methods. In the U.S., UHPC compressive strength is usually tested in accordance with ASTM C39 "Standard Test Method for

Compressive Strength of Cylindrical Concrete Specimens” [76], along with ASTM C1856. One major change that ASTM C1856 makes to the ASTM C39 method is the reduction of specimen size (3 × 6 in. instead of 4 × 8 in.). This is partially due to limitations on the loading capacity of some compression testing machines. It also serves to reduce the amount of expensive UHPC that is wasted for testing. Because UHPC has a very small maximum aggregate size, the specimen size reduction does not affect results as much for UHPC as it would for normal concrete. As described in ASTM C39, the loading rate for normal a concrete cylinder would be 35 ± 7 psi/s, but since UHPC has a significantly higher compressive strength, ASTM C1856 specifies a loading rate of 145 ± 7 psi/s in order to decrease the testing time (ASTM C1856-17, 2019). Both ends of UHPC specimens need to be ground because elastomeric pads are not suitable for use above 12 ksi, and bonded sulphur caps are weaker than the UHPC concrete.

1.6. Durability

UHPC is reported to have excellent performance against deterioration mechanisms that involve water or ion ingress into concrete. These mechanisms include freeze-thaw deterioration, deicer-salt scaling, abrasion, alkali-silica reaction, sulfate attack, chloride penetration, and carbonation. This durability is thought to come from the very low connected porosity of UHPC [77], [78].

1.6.1. Freeze-thaw resistance

Air entrainment is typically used in concrete to provide protection against freeze-thaw deterioration. It is precluded from being used in UHPC however because it would unacceptably reduce the strength. In contrast to normal-strength concrete without air entrainment, UHPC has been shown to have excellent freeze-thaw durability. The low permeability and porosity of UHPC are thought to keep the concrete from becoming critically saturated [79].

Several studies have been conducted to investigate the freeze-thaw performance of UHPC. Ahlborn et al. performed freeze-thaw cycling on UHPC in accordance with ASTM C666, procedure B (freezing in air, thawing in water) for 300 cycles with no degradation measured [80]. Similarly, Acker and Behloul reported that UHPC showed no degradation after 400 cycles of freezing and thawing [81]. Russell and Graybeal showed that untreated UHPC specimens and UHPC specimens subjected to steam curing showed at least a 96% relative dynamic modulus of elasticity after 690 cycles of freeze-thaw conducted according to ASTM C666 procedure A-freezing and thawing in water [11]. Another study measured the resistance of UHPC to freeze-thaw in the presence of a NaCl solution, conducted according to CEN/TS 12390-9, that showed an extremely low mass loss after 112 freeze-thaw cycles [82]. Another study performed on UHPC with 2.5% steel fibers found a 15.8% increase in loading capacity after 600 freeze and thaw cycles [83]. Freeze-thaw testing of concrete made with locally produced materials having a 14,100-psi compressive strength showed no freeze-thaw damage up to 600 cycles. Between 600 and 1500 cycles, minor damage was observed, resulting in exposed steel fibers and reduced first-cracking strength [84].

UHPC has been found to have excellent field durability in cold climates. At the Cattenom power plant in France, UHPC was used to replace some of the beams. After six years of exposure in the aggressive environment with natural freeze-thaw cycles, there was no noticeable degradation of the beams [85]. In another case, UHPC samples were placed at the Treat Island, Maine exposure site maintained by the U.S. Army Corps of Engineers. Tide levels vary by as much as 22 feet at this site with the temperature during the winter ranging from -10 to -37°F (-23 to -38°C), making this site an ideal place to test UHPC performance. After several years of exposure and hundreds of freeze-thaw cycles, no evidence of deterioration or mass loss was seen on any samples [86].

While theories exist on the mechanism responsible for UHPC freeze-thaw durability, testing is needed to validate these theories. This will provide guidance to mixture design and test methods required for freeze-thaw performance. UHPC testing performed to date has mostly focused on concrete with compressive strength above 22 ksi. It is also not known at what strength level UHPC transitions to excellent freeze-thaw performance. ASTM C1856 requires UHPC freeze-thaw testing to be conducted according to ASTM C666 Procedure A for at least 300 cycles or until its relative dynamic modulus of elasticity reaches 90%. ASTM C666 requires the concrete to be cured in limewater for 14 days before testing, or 2 days if saw-cut from hardened concrete. No changes are recommended for UHPC curing or saturation level. If UHPC freeze-thaw durability comes from the low degree of saturation, this may not be reliable long term.

1.6.2. Scaling resistance

UHPC has been shown to have excellent deicer-salt scaling resistance. The mechanism is not known, but it is possible that the high material tensile strength could help resist fractures that occur in the surface from the glue-spall effect [87]. Graybeal tested the salt scaling resistance of UHPC mixes and found no damage after 215 cycles [88]. Another study compared UHPC and normal-strength concrete. The mass loss due to surface scaling was > 1000 g/m^2 for normal-strength concrete compared to 7 g/m^2 for UHPC mixes after 1000 freezing and thawing cycles [85]. Another study showed that UHPC exhibited 100 g/m^2 mass loss after 56 cycles, or only 6.7% of the test limit [89]. Salt scaling performance has been measured for some non-proprietary UHPC mixes that were subjected to 50 cycles of freezing and thawing, and there was no visible deterioration observed, resulting in a zero rating [90].

1.6.3. Resistance to alkali-silica reactivity

Concrete can experience deterioration from Alkali Silica Reaction (ASR) when reactive aggregates are used in concrete with a sufficiently high alkali loading. Due to the high content of cement and consequent alkali loading in UHPC mixes, it is important to evaluate the risk of ASR. One study with very-high-strength concrete made without SCMs found that ASR could occur, even at 0.2 w/cm. That study found however that when the mixture used fly ash, it was able to suppress the reaction. UHPC made with silica fume has shown excellent ASR resistance [91]. The ASR risk of UHPC was tested in one study in accordance with ASTM C 1567 “Standard Test Method for Determining the Potential Alkali-Silica Reactivity of Combinations of Cementitious Materials and Aggregate (Accelerated Mortar-Bar Method)” [92]. In this test, UHPC samples are immersed in a 1 N NaOH solution at 176°F (80°C). No expansion or deterioration of UHPC was found in this testing [82]. Graybeal also used an accelerated mortar bar test to measure ASR risk and found expansion below the nonreactive threshold limit of 0.10% [17]. Moser reported that no increase in expansion for UHPC samples could be measured after 600 days, and the expansion was below the threshold limit [93]. Sawab et al. tested some UHPC mixes containing quartz sand and compared the specimens with controls containing river sand. The results indicated that the control specimens fell into the potentially deleterious category, while UHPC specimens showed no expansion [94]. In summary, the results from several studies indicate that UHPC made with SCMs should not experience ASR, especially if steam-curing is applied.

1.6.4. Sulfate resistance

Very limited research has been conducted on UHPC sulfate resistance, mainly because UHPC risk to sulfate attack is generally considered minimal. One study was performed, however. Three UHPC prisms of 1.6 × 1.6 × 6.3 in. (40 × 40 × 160 mm) were immersed in a sodium sulfate solution

Na_2SO_4 (16 grams of SO_4^{2-} per liter) for 500 days, and the length was measured regularly. The results indicated no expansion or deterioration of the samples. [82]. These results demonstrate how the very low permeability of UHPC keeps sulfate ions out of the concrete, significantly reducing the risk of deterioration from external sulfate attack.

1.6.5. UHPC transport properties

The ability of concrete to resist fluid ingress through the specimen is an important indicator of its durability. Penetration of concrete by fluids containing deleterious ions occurs through pores and the capillary connections between the pores. Ion transport occurs inside concrete by different mechanisms such diffusion due to concentration gradients, pressure gradients from external sources, and capillary action (sorptivity) [95].

1.6.5.1. Electrical tests

Electrical properties of concrete have been used for many years as a quality indicator. Electrically conductive pore solution can fill concrete pores, making it electrically conductive. The concrete electrical resistivity, or inverse of conductivity, is dependent on both the pore system and the pore solution conductivity, and can be normalized by the pore solution resistivity ρ_0 ($\Omega\cdot$m) to give an empirical material pore system index called the formation factor *F*, as shown in Equation 7 [96]:

$$\frac{\rho_T}{\rho_0} = F \qquad \text{Equation 7}$$

Where: ρ_T is the concrete electrical resistivity ($\Omega\cdot$m)

The formation factor is independent of specimen size or shape, and it is related to the pore system as the inverse of the product of the concrete porosity volume $\emptyset$ and connectivity β, as shown in Equation 8 [97], [98]:

$$F = \frac{1}{\emptyset\beta} \qquad \text{Equation 8}$$

The Nernst-Einstein relationship can also be used to relate *F* and the concrete electrical resistivity to the concrete bulk effective diffusion coefficient *D* (m^2/s), as shown in Equation 9 [96], [99]:

$$\frac{\rho_T}{\rho_0} = F = \frac{D_o}{D} \quad \text{Equation 9}$$

Where: D_0 is the self-diffusion coefficient (m^2/s)

Equation 9 shows how the concrete resistance against chloride penetration can be proportional to the concrete electrical properties. This relationship is what allows concrete electrical tests to be used for concrete quality tests.

The concrete pore system, pore solution conductivity, and consequently electrical resistivity are highly dependent on the concrete mixture characteristics such as cementitious material composition, water-to-binder ratio, and degree of hydration [98]. As the concrete hydrates with time, the microstructure and pore solution can also be significantly changed due to environmental conditions [98].

One study attempted to measure the formation factor on UHPC using a resistivity meter. They cured the samples in a simulated pore solution after 7 days of sealed curing. They assumed that the sample pore solution came into equilibrium with that of the simulated pore solution. This is questionable because of the very low transport properties of UHPC. Additionally, it is unlikely that the UHPC was saturated during that period of time, potentially giving unconservative transport properties. Twenty-eight-day results showed that the formation factors they measured are considerably higher than normal-strength concrete. In addition, the results indicated an estimated time for corrosion initiation of 210 years for UHPC mixes [100]. Steel fibers are electrically conductive and greatly alter the measured values, even though they would not change the actual transport properties.

1.6.5.1.1. Surface and Bulk Resistivity

In order to calculate the formation factor, the concrete electrical resistivity must be measured. Surface resistivity can be used to evaluate the electrical resistivity of a saturated concrete cylinder to provide an estimation of its permeability [101]. One of the most common techniques for measuring the surface resistivity is a four-probe technique. In this technique, four equally-spaced electrodes are located on the concrete surface to measure the potential difference caused by the applied current [102]. The Surface electrical resistivity can be calculated by using Equation 10:

$$\rho = K \times R = K \times \left(\frac{V}{I}\right) \qquad \text{Equation 10}$$

Where: ρ is the concrete surface resistivity (Ω-cm)
R is the measured resistance (Ω)
V is the voltage measured between two inner probes (V)
I is the applied current by the two exterior probes (A)
K is the geometry factor

It is very important to apply an appropriate geometry factor K that converts the resistance to a resistivity. Many commercial surface resistivity meters such as the Proceq Resipod automatically apply a correction factor of 2πa. The geometry correction factor to obtain the resistivity can be calculated using the Equation 11:

$$K_{surface} = \frac{2\pi a}{1.10 - \frac{0.730}{d/a} + \frac{7.34}{(d/a)^2}} \qquad \text{Equation 11}$$

Where: a is the probe tip spacing (cm)
d is the specimen diameter(cm)
L is the specimen length(cm)
$K_{surface}$ is the geometry correction and it is only valid for specimens with $d / a \leq 4$ and $L / a \geq 5$

The bulk resistivity test uses the same equipment (4-pronged Wenner probe) as surface resistivity to measure the resistance of the cylinder with the probe tips attached to conductive plates placed on the end of the cylinder [103]. Saturated sponges or conductive gel are typically used between the conductive plates and the ends of the cylinder, as shown in Figure 16. The bulk resistivity can be calculated using Equation 12:

$$\rho = R_{cylinder} \times K \qquad \text{Equation 12}$$

Where: ρ is the resistivity of the concrete (Ω·cm)
$R_{cylinder}$ is the calculated bulk resistance (Ω)

K is the geometry factor, which is the ratio of the cross-sectional area A (cm^2) to the length of the specimen L (cm)
a is the probe tip spacing (cm)

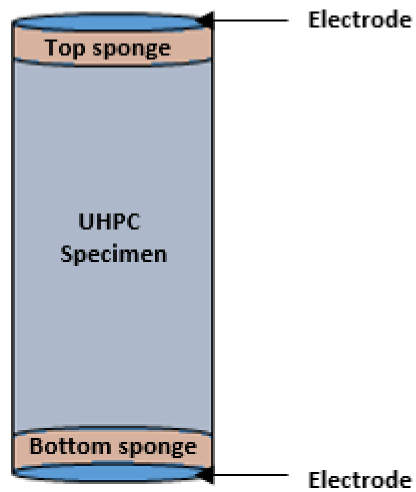

Figure 16: Bulk resistivity set-up

UHPC resistance to chloride penetration was evaluated using the surface and bulk resistivity test methods. The electrical resistivity measurements were within the ranges of very low to negligible at 28 days. This is due to the very dense microstructure of UHPC [4]. The results illustrated that these tests might be able to be used with mixes having fibers since the fibers most of the time do not touch to create a conductive path along the entire length of the specimens since they are randomly dispersed except when some alignment due to material flow during placement cannot be avoided.

1.6.5.1.2. Rapid chloride permeability test:

ASTM C1202 "Electrical Indication of Concrete's Ability to Resist Chloride Ion Penetration" [104] has been commonly used for determining the transport properties of UHPC. This test method, typically referred to as the rapid chloride penetration test (RCPT), involves at least two days of specimen preparation after the desired curing procedure. The samples need to be cut into 2-in. thick slices and placed in a vacuum desiccator with both ends exposed. The vacuum is maintained for three hours in the desiccator, and then the desiccator is filled with de-aired water and maintained for an additional hour. After that, the samples should be allowed to soak for 18 ± 2 hours. The exposed sides of 2-in. thick samples are sealed to avoid any moisture loss, and then placed inside a testing cell with one side of the cell filled with 3.0% sodium chloride (NaCl) and the other side filled with 0.3M sodium hydroxide (NaOH) solutions, as shown in Figure 17. The electrical charge passed between the electrodes is integrated with time using readings taken every 30 minutes during the six-hour testing period [105]. Even though this test has been adopted as a standard test, there have been number of criticisms of this technique related to the high voltage used, temperature rise of the specimen, and the effect of admixtures that may mislead the results [106], [107].

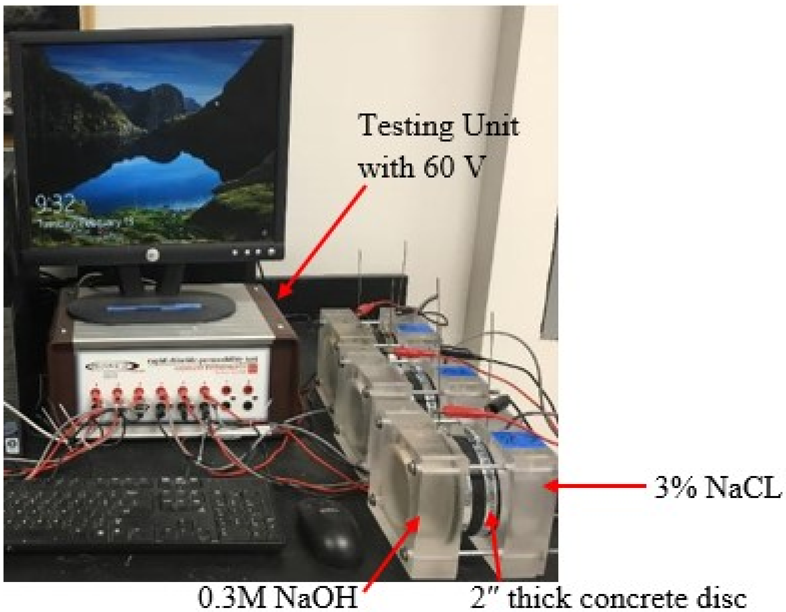

Figure 17: RCPT test set-up

ASTM C1856 requires that ASTM C1202 only be used with UHPC that does not contain metallic fibers [46] because the fibers will conduct electricity but not significantly change the chloride ingress. ASTM C1856 also warns that UHPC that has been heat-cured may give values very close to zero Coulombs. It is unknown what a measurement close to zero means in terms of pore connectivity. Additionally, since most UHPC is reinforced with steel fibers, the applicability of this test for qualification or quality control testing may be limited unless it can be shown otherwise. Graybeal tested some UHPC mixes with steel fibers, and the results showed a possibility of using this test provided no conductive path is created between the two ends of the specimens [4]. More work is needed to determine how much an effect the fibers actually have on the measured values.

Studies conducted on UHPC with ASTM C1202 have shown that the electrical conductivity is low. El-Tawil et al. tested two UHPC mixes with three different fiber volume contents (0.5%, 1.0%, and 1.5%), and reported that the penetration of chlorides was negligible [90]. Graybeal tested some UHPC mixes having different percentage of steel fibers (2 – 4.5% by volume) using ASTM C1202 and applied two different curing regimes: lab temperature and steam curing. The charge passed was found to be negligible for both steam-cured and untreated specimens after 56 days [88]. In samples made using 0.2 w/cm and 20% replacement of cement with silica fume, it was observed that only 64 Coulombs was passed, which is considered to be negligible according to ASTM C1202 [108].

1.6.5.1.3. Rapid chloride migration test

NT Build 492 test uses an electrical voltage to accelerate chloride migration into a concrete specimen [109]. In this test method, a 2-in. thick concrete sample is exposed to a 10% NaCl solution on one side and a 0.3 N NaOH solution on the other, as shown in Figure 18. The test is set for 30 Volts, then the voltage and test duration can be adjusted based on the initial current. After the test is done, the concrete specimen is split in half, and 0.1 M silver nitrate is applied to measure the chloride penetration. The non-steady state migration coefficient is calculated using Equation 13:

$$D_{nssm} = \frac{0.0239(273+T)L}{(U-2)t}\left(x_d - 0.0238\sqrt{\frac{(273+t)Lx_d}{U-2}}\right) \quad \text{Equation 13}$$

Where: D_{nssm}: non-steady-state migration coefficient, $\times 10^{-12}$ m^2/s;
U: absolute value of the applied voltage, V;
T: average value of the initial and final temperatures in the anolyte solution, °C;
L: thickness of the specimen, mm;
x_d: average value of the penetration depths, mm;
t: test duration, hour.

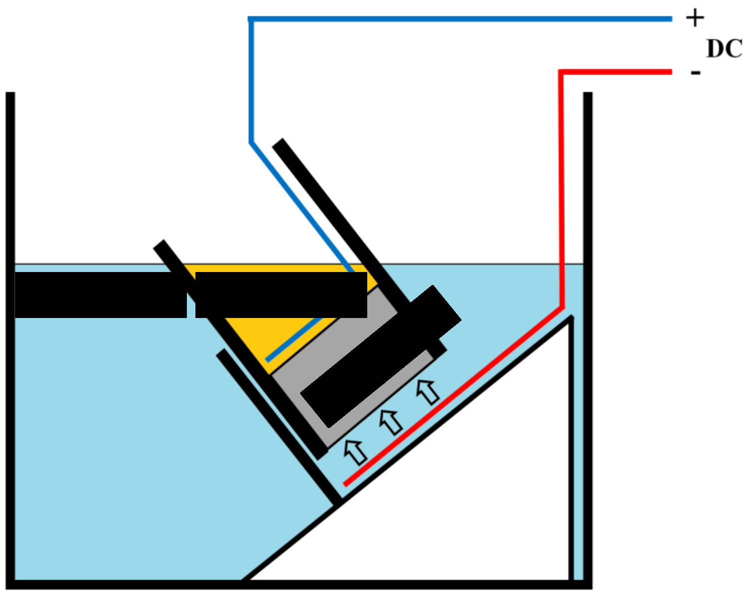

Figure 18: NT Build 492 test set-up

This test has been modified to measure the chloride penetration through UHPC samples. Vincler et al. have modified the test; these modifications include increases in the volume of the solution to 2.7 L and the voltage to 70 V [110]. These modifications reduce the heat issues and accelerate the test time. Based on the results, the depth of chloride penetration for the UHPC samples did not reach 0.2 in. (5 mm), and the diffusion coefficient was 10^{-15} m^2/s. They concluded that the proposed test gives accurate results for the diffusion coefficients when compared to 5-year chloride exposure. Mosavinejad et al. tested the durability of some UHPC mixes using NT Build 492 [111]. They ran the test for 96 h since the initial current was below 5 mA. The results showed the UHPC has an extremely high resistance to chloride penetration. Rafiee compared the results of UHPC, HPC, and ordinary concrete tested using NT Build 492 [112]. There was no chloride penetration for UHPC, compared to 7.5 mm for HPC, and 31 mm for the ordinary concrete.

NT Build 492 shows excellent promise for qualifying UHPC mixtures based on their resistance to chloride penetration. Testing is needed to determine the effect of steel fiber inclusion on the results, and how to interpret results with such a low chloride intrusion.

1.6.5.2. Chloride ion diffusion

Chloride penetration in UHPC has been found to be much lower than high-performance concrete (HPC) and normal-strength concrete [113]. ASTM C1556 "Standard Test Method for Determining the Apparent Chloride Diffusion Coefficient of Cementitious Mixtures by Bulk Diffusion" [114] is a common method for determining the concrete chloride diffusion coefficient. In this method, concrete specimens are split into two parts, the 3-in. top part of a 4 × 8 in. cylinder is sealed with epoxy from all sides except the finished surface and vacuum-saturated with $Ca(OH)_2$ for at least 18 hours, then submerged in sodium chloride solution for at least 35 days. Most high performance concrete are exposed to chlorides for much longer time, usually one year. The bottom part of the specimen is used to measure the concrete initial chloride concentration. The chloride content for both the top and bottom parts are measured using titration as described in ASTM C1152 [115]. The chloride diffusion coefficient can then be calculated by fitting a calculated chloride profile to the measured chloride profile.

Bulk chloride diffusion testing on UHPC has shown that it has excellent resistance to chloride penetration. In one study UHPC mixes were exposed to chloride solution for 90 days, and then the top surface of the specimens was ground off. The depth of chloride penetration was found to be 0.08-0.12 inches (2-3 mm), and the chloride diffusion was found to be as low as 1×10^{-13} m^2/s compared to normal concrete at 5×10^{-12} m^2/s to 5×10^{-11} m^2/s [116]. This test may prove to be impractical for routine UHPC testing because of the length of time required for the concrete to be ponded for any measurable amount of chlorides to penetrate.

1.6.5.3. Water absorption

When water is absorbed into partially saturated concrete, it can bring with it chlorides or other aggressive ions [117]. ASTM C1585 "Standard Method for Measurement of Rate of Absorption of Water by Hydraulic- Cement Concrete [118]" is commonly used to determine concrete water absorption. In this method, 2- × 4-in. concrete disks are conditioned for not less than 18 days. The conditioning period begins with placing the samples in a chamber maintained at a temperature of 122°F (50°C) and a relative humidity of 80% for three days. After that, the samples are placed in a sealed container at a controlled temperature of 73 ± 3.6°F (23 ± 2°C) for at least 15 days to allow the sample moisture content to come to a constant value throughout the sample thickness. The sample bottoms are then exposed to water by placing them on supports in water, with the water depth at 0.079 ± 0.039 in. (2 ± 1 mm) from the sample bottom. The samples are weighed periodically for 8 days to measure the water uptake. The absorption of the samples can be determined using Equation 14:

$$I = \frac{m_t}{A \times d} \qquad \text{Equation 14}$$

Where: I is the absorption (mm)
m_t is the change in mass of the specimen (g) at time t
A is the exposed area of the specimen (mm^2)
d is the density of the water (g/mm^3)

The slope of absorption can be determined for the primary and secondary absorption rates. The primary absorption rate is the slope of the best-fit line to the absorption for the first 6 hours. The secondary absorption rate is the slope of the best-fit line to the absorption for the first week of the test.

BS EN 12390-8 is a common method used for determining the depth of water penetration under pressure in hardened concrete [119]. According to this method, after demolding, the surface of specimens that are going to be exposed to water pressure should be roughened and cured at least 28 days. A water pressure of 72 ± 7 psi (500 ± 50 kPa) is applied for 3 days, then the specimens are split into halves, and allowed to dry slightly until the water penetration front can be clearly seen. The maximum depth of penetration is then measured to the nearest mm.

The relative humidity of the samples considerably affects the results and can lead to misinterpreting the actual absorption behavior. In fact, samples conditioned at a 50% relative humidity showed almost six times of total absorption higher than samples conditioned at 80% relative humidity. Therefore, the sample curing history and conditioning should be taking into account for more reliable and less variations in the results- especially for field samples [120]. A comparison was made between conditioning samples with two different procedures, conditioning the samples as mentioned in ASTM C1585, and placing the samples in an oven at 140°F (60°C) until constant mass. It was concluded that drying the samples at 140°F (60°C) gave more reliable measurements for the sorptivity testing [121].

UHPC has been shown to have very low water absorption, mostly because it has such low porosity. UHPC has only 1-2% capillary pores by volume [122]. Roux et al. made two UHPC mixes: one was table-vibrated, and the other was produced with a pre-set pressure of 8.7 ksi. The water absorption values for both mixes were observed to be less than 4.5×10^{-4} lb/in.^{2}. This is due to the absence of capillary porosity [117]. A similar trend was observed when comparing the water absorption of UHPC to HPC (Dili & Santhanam, 2004). O'Neil et al. compared UHPC and HPC water absorption and reported that for UHPC, the rate of water absorption according to the EN 13369 standard was seven times lower [123]. Another study looked at the effect of micro fillers on UHPC water absorption. At an age of 90 days, very-high-strength concrete made with coarse aggregates and ultra-high-performance concrete mixes had low water absorption due to the low level of capillary pore connectivity. The water absorption values measured according to the EN 13369 standard are presented in Table 1, where the silica fume gives the lowest values for both mixes (0.7%, and 3.3%) [124]

Table 2: Water absorption (%) of UHPC and VHPC at age of 90 days [124]

	Silica fume	Metakaolin	Phonolith	Pulverized fly ash	Limestone micro filler	Siliceous micro filler
UHPC	0.7	1.9	2.2	3.2	2.8	1.6
VHPC	3.3	4.0	4.2	4.3	4.2	4.1

Fibers have been found to influence the water absorption amount. The high content of steel fibers in UHPC tends to decrease water absorption, unlike polypropylene fibers, which tend to increase the water absorption [125].

Overall, water absorption shows significant promise for use as a qualification test for UHPC because it includes the effects of pore connectivity and tortuosity. If pressurized in some way like the EN 12390-8 test, it could be performed in just a few days and could differentiate UHPC where chlorides cannot penetrate more than 0.39 in. (10 mm) at a slow rate.

1.6.5.4. Mercury intrusion porosimetry (MIP) test

MIP is a common test used for characterizing the porosity and the size distribution of capillary pores in cement paste specimens. The test procedure usually involves breaking the samples into small pieces, stopping the hydration through a solvent exchange, removing the moisture by vacuum until a constant weight is achieved, and using high pressure to fill the pores with mercury [126].

MIP is based on the physical phenomenon that as a non-wetting liquid, no capillary absorption will occur. Mercury encases the sample and will only penetrate capillaries when high pressure is applied. Pore size can be determined from the applied pressure, using an assumed pore geometry [127], [128]. The pore shapes are assumed to be cylindrical, and the relationship between the pore size and the applied pressure is given by Washburn equation, as shown in Equation 15 [127], [128]:

$$\Delta P = \frac{2\,\gamma\,cos\,\theta}{r_{pore}} \qquad \text{Equation 15}$$

Where: ΔP is the pressure difference across the curved mercury interface (Pa)
γ is the surface tension of mercury (N/m)
θ is the contact angle between the solid and mercury
r_{pore} is the resultant pore size (m)

MIP has some drawbacks. The assumed cylindrical pore shape is much different than the shape of the actual pores. During drying, the pore walls could be damaged, and under high pressure the mercury could break through thin or damaged walls and alter the pore structure [126], [129].

Vincler et al. have performed MIP on some UHPC mixes with 1% fibers. For most of the samples, the intruded pore sizes were about 2 nm [110]. A study by Cheyrezy et al. used MIP to demonstrate the very low porosity of reactive powder concrete (RPC). The cumulative porosity ranged primarily from 3.75 nm to 100 μm and did not exceeded 9% in volume [34]. Kang et al. used MIP on some UHPC samples with different heat curing. They concluded that the increase in temperature made the UHPC pore structure finer, less than 100 nm [130]. The incorporation of nano-SiO_2 in UHPC was found to lead to a decrease in the amount of capillary pores as measured by MIP [131]. UHPC in another study was found to have a total porosity of 7.88%, compared to 12.69% for normal concrete, confirming that UHPC has a really small open-pore volume [132]. This pore system difference measured by MIP seen could serve as a good measure of the concrete's ability to keep out water and chlorides.

1.6.6. Carbonation

Carbonation is the reaction of cement hydration products with carbon dioxide (CO_2). The reaction of carbon dioxide from the atmosphere with calcium hydroxide in solution forms calcite ($CaCO_3$), as shown in Equation 16.

$$Ca(OH)_2 + CO_2 \longrightarrow CaCO_3 + H_2O \qquad \text{Equation 16}$$

This reaction can reduce the alkalinity of concrete, leading to the destruction of the passive layer on reinforcing steel. However, since the UHPC has a very low w/cm and has a very dense structure, UHPC carbonation rates are extremely low. It was found that there was no carbonation of UHPC specimens that were exposed to 5% CO_2 for 42 days and to 100% CO_2 for 90 days, but some penetration was reported in later ages of exposure [133]. In another study, UHPC prisms with a cross-section of 4 × 4 in. (100 × 100 mm) were oven-dried at 120°F (50°C) for the first two weeks and then stored in a 1% CO_2 atmosphere for accelerated aging. The results indicated that the carbonation depth was 0.06 to 0.08 inches (1.5 mm to 2 mm) after one year of exposure [116]. In one study, composite reinforced concrete (CRC) beams were made by Aarlborg Portland. These beams had a low w/cm between 0.15 and 0.2, 6% by volume of steel fibers, and 20-25% cement replacement by silica fume. After being exposed for 16 years to Madrid's climate, where the temperature ranges between 20 and 90°F (-6 to 32°C), the carbonation depth was measured. The results showed that the beams were very resistant to carbonation penetration, and the depth of carbonation recorded was less than 0.039 inch (1 mm) from the surface. [134]. Carbonation performance of Ductal® with 2% of steel fibers was compared to that of very high-performance concrete. It was reported that after four months of an accelerated carbonation test, the carbonation penetration depth of Ductal® was below the limit of detection of around 0.020 inch (0.5 mm) [124].

1.6.7. Abrasion resistance

Abrasion resistance is the "ability of a surface to resist being worn away by rubbing and friction" [135]. UHPC has excellent abrasion resistance and has begun to be used in hydraulic structure repair because of its excellent abrasion resistance [136], [137]. Abrasion resistance is a function of the material surface hardness and material elasticity to prevent brittle cracking [138]. Materials with high hardness are brittle and abrasion can induce brittle cracking of the surface leading to high wear. The matrix has to have some elasticity/plasticity so that it can hold aggregate particles in place without fracturing. The very-high-strength of UHPC and steel fiber reinforcement contributes to this resistance [139].

Several test methods have been developed to measure abrasion resistance for normal-strength concrete. ASTM C418 measures the concrete wear after sandblasting to simulate air- and water-born abrasive damage [140]. ASTM C1138 was developed by the U.S. Army Corps of Engineers originally and uses steel ball agitation in water to measure concrete resistance to erosion-abrasion [141]. ASTM C944 simulates concrete wear under steel-tire impact. In this method, a rotating cutter is used to abrade the surface of concrete samples in a given time. The cutter has a 22 ± 0.2 lb weight placed on it as it rotates to increase the friction force [142]. ASTM C1856 modifies ASTM C944 for the high UHPC strength and abrasion resistance. For UHPC, it is recommended to use 44 ± 0.4 lb instead of the normal load to accelerate the test. It was shown that the mass loss for UHPC was linear with the weight, allowing for this test acceleration without affecting the results [90].

Several studies have been performed to demonstrate the benefits of UHPC on abrasion resistance. Reactive powder concrete (RPC), a predecessor material to UHPC, was examined for use in overlays. It was found that the RPC had eight times the abrasion resistance of normal-strength concrete and four times that of high-strength concrete when cylinders were tested for 1000 cycles [143]. The type of curing has been found to affect UHPC abrasion resistance. Graybeal and Tanesi compared UHPC abrasion resistance after four types of curing: steam, ambient air, tempered steam, and delayed steam curing. The results indicated that the values for ambient air-cured specimens were between 1.1 g to 2.1 g of weight loss, which is high compared to 0.1 to 0.3 g weight loss for the steam-cured specimens [144]. The steam-curing treatment dramatically enhances the abrasion resistance of UHPC due to increasing the degree of hydration and the strength [144]. Aggregates also play a significant role in the UHPC abrasion resistance. When comparing different UHPC mixes, it was found that UHPC with coarser aggregate showed a 50% higher abrasion loss than UHPC with no coarse aggregate [145].

1.6.8. Field performance

In 1995, UHPC was used for the first time in North America, on a bridge in Quebec, Canada. The 197-foot (60-m) long bridge showed no deterioration, despite exposure to aggressive marine environment [146]. In 1997, three UHPC samples were subjected to daily tides and freeze-thaw cycles at Treat Island to monitor long-term durability. They measured the chloride penetration and found that chlorides did not penetrate farther than 0.39 inch (10 mm) into the concrete, even after 15 years of exposure [86].

1.7. Non-destructive evaluation methods

Non-destructive evaluation (NDE) which is also commonly referred to as non-destructive testing (NDT) or non-destructive inspection (NDI), is an approach for testing materials or structural members. The process is used to determine the health or characteristics of the material that is being studied. This approach contrasts with widely-used destructive testing, where the structure is placed under load or in other adverse conditions for study or to determine causes of failures [147]. As a result, NDE/NDT/NDI is necessary when the structure is intended to remain in use. It allows the health of the system to be evaluated and maintenance or rehabilitation of such structure to be carried out [148], [149]. NDE is also used to estimate the life expectancy of structures, such as bridges and buildings, for the purpose of planning and improvement [149]. NDE could provide a way to inspect structural members made with UHPC to ensure fiber distribution and orientation specifications are met. A discussion of NDE methods applicable to concrete is given.

The oldest and still most common NDE method is visual inspection [148], where the structure is physically examined for cracks and faults that can be seen on the surface. This approach is relatively inexpensive and requires relatively little training. The method is useful as cracks on the surface, or even delaminations, that are observable from visual inspection are a clear sign of problems in the inspected structure [148]. The disadvantage, however, is the fact that many faults are not visually observable on the surface of the material. Many serious faults often start deeper in the material [150].

For concrete, there are some challenges associated with the visual inspection, such as the existence of microcracks that are not easily visible. Also, the person inspecting needs to know what exactly to look for [150]. In addition, some of the areas that need inspection are often not accessible or are only accessible from one side of the concrete structure. The possibility of damage from an inaccessible surface means visual inspection cannot accurately assess the structure.

To address the disadvantages of visual inspection, various NDE methods have been developed and continue to be developed as the need for more robust and more informative inspections grow. In this document, five broad categories of non-destructive evaluation will be discussed: electrical [147], electromagnetic [148], thermographic [150], radiographic [150], and sonic/ultrasonic [148]. How each of these analytical methods are used to inspect concrete, their advantages, and their disadvantages will be described. A rigorous review of ultrasonic inspection techniques, which are a focus of this project, will be performed.

1.7.1. Sonic and ultrasonic nondestructive evaluation methods

These methods involve the transmission and receiving of mechanical stress waves through a material at sonic (20 Hz – 20 kHz) and ultrasonic (typically greater than 20 kHz) frequencies. They are generally non-invasive contact or non-contact methods that analyze sounds and sound echoes/reflections and how different materials respond to them.

1.7.1.1. Impulse-Response Method

The impulse response method is the sonic/ultrasonic method that requires the fewest devices to implement and is commonly used in practice. Its use is codified in ASTM C1740 [151]. The method uses a calibrated rubber-ended hammer with a load cell [151] connected to the data acquisition system that induces elastic waves in the structure under test. This is used to generate the force spectrum. The elastic wave propagation in the structure is picked up by a geophone [148] (pickup microphone) that generates a velocity spectrum output of the received signal due to the impact force from the hammer and subsequently amplifies it before signal processing is performed [152]. The signal processing is done by taking the fast Fourier transform (FFT) of the signal and the resulting velocity spectrum divided by the force spectrum to get a transfer function called the mobility of the test, which is given in (m/s)/N [152]. The mobility is plotted against frequency, which is a measure of the flexibility and the elastic modulus of the structure/material.

One of the sewer tunnels west of the pumping stations in St. Louis, Missouri [152] was tested with impulse-response at four test points after the flooding from the Mississippi river in 1993. It was successfully shown that three points were in good condition with no voiding behind the brick lining and one was very weak and was subsequently reinforced by replacing the defective portion.

The advantage of this method is the ease with which it can be implemented because of the simplicity of the equipment involved. One major drawback is the poor defect location precision and the complexity of interpreting the results that requires some understanding of how the material should respond [147].

1.7.1.2. Impact-echo method

The impact-echo is similar to the impulse-response method. In fact, some literature consider them the same [148].The two methods are different in that the impact-echo method typically operates at a much higher frequency range, typically around 10 kHz to 150 kHz [147], [153]. The higher frequencies occur from the impact because of the diameter of the impacting device is reduced [147]. When the data is collected, an FFT is performed on the received elastic wave from the pickup device. A frequency response function is made from the signals, and the resonant frequency peaks correspond to the thickness or depth of the faults in the structure. If the depth of the structure is known, incorrect depths will correspond to a fault.

This is a widely accepted and used method because of its ease of testing, since very simple tools are needed for the impact, and success with identifying voids in ducts [148]. Its use is codified in ASTM C1383 [154]

Recently, artificial neural networks have been used in the impact-echo analysis [155]. The impact-echo method trains the network with a set of input-output data, where the input is impact-echo data and the output is the presence of cracks in the structure. The neural network is then able to give appropriate output data for every input variable after training with back propagation [155]. Concrete conditions have also been determined using extreme learning machines [156] using techniques that learn from the impact-echo data obtained.

The advantage of this method is that it is a simple way of testing without the need of coupling the sensor to the base because the pickup microphone is air-coupled [147]. The drawback, however, might arise from the inability to sometimes interpret the results accurately because of possible sensitivity issues in the transducer or even low frequencies resulting in the indistinguishability of the defect areas [148], [155].

1.7.1.3. Ultrasonic method

The ultrasonic method uses ultrasonic waves (typically greater than 20 kHz frequency) to probe concrete structures. Its use is codified in ASTM B548 [157].This data is gathered in three different forms: A-scans, B-scans, and C-scans. A-scans show a one-dimensional image of the structure by measuring reflected signals over time from the structure and plotting it against its amplitude [158]. If the wave velocity is known, the time axis can be converted into depth into the material. A B-scan is a “slice” of the vertical profile of the structure [159]. The B-scan shows a two-dimensional image across time and location. The color of the image usually corresponds to the amplitude at the time and location. A C-scan provides the surface “snapshot” of the structure. The C-scan shows a two-dimensional image across horizontal locations and vertical locations. The color of the image usually corresponds to the maximum amplitude across some time range (or gate).

The three different scans of the structure can also be combined in a number of ways to form a 3-D analysis of structures [158]. This method has gained a lot of attention and research over the years because of its versatility in showing defects deep inside the structure. A piezoelectric transducer is used to generate sounds that are greater than 20 kHz or the threshold of human hearing. This generated wave excites the structure typically using bulk waves. The waves are then transmitted through the structure and then reflected. The reflected signal is then processed using different algorithms, one famous algorithm being the synthetic aperture focusing technique (SAFT) algorithm [160]. A color map is then generated based on the different densities that the structure is made of. Faults and delaminations can then be seen as these typically have an earlier arrival [161] than the back of the structure for example, and these will stand out in the image of the structure that is generated.

The advantage of this method is that a lot of details can usually be obtained from the scan of the structure revealing things like flaws and voids with proper interpretation [147], [148]. Impedance matching ensures that the intensity of the wave is not attenuated by the air gap that exists between the transducer and the structure without proper coupling. One major drawback of this method is its time consuming nature, which limits the speed at which tests can be carried out [159].

1.7.1.4. Ultrasonic pulse velocity method

The ultrasonic pulse velocity method [162] is one of the oldest and most widely accepted sonic/ultrasonic methods for concrete testing. Its use is codified in ASTM C597 [163]. It is effective for non-destructive testing and evaluation of the quality and uniformity in concrete samples. It is typically used to determine compressive strength and the elastic modulus of concrete [164]. Figure 19 shows an example of setup. The setup uses a transmitter to send an ultrasonic wave, a receiver to receive the wave, a pulse generator that generates the wave, and a device to amplify and display the received signal. The amplification device can be standalone or coupled with other devices. When a time-varying mechanical force excites a semi-infinite solid like a concrete surface, three types of waves are typically propagated, the fastest of which is the longitudinal wave, also called P-wave or compression wave [165], [166]. The secondary wave is called the shear, also called S-waves [166], [167]. The third wave is the surface wave [168]. The time of arrival is recorded as the difference between the time when the excitation begins and when the first wave arrives. This is used to calculate the compression wave velocity by dividing the path length of the wave through the concrete by the time of travel through the concrete. From the compression wave velocity, we can compute the Young's modulus [148] and other desired properties [164]. The health or quality of the concrete can also be linked to the velocity of the wave through the concrete, where generally we want values greater than 3500 m/s to indicate at least a good quality concrete.

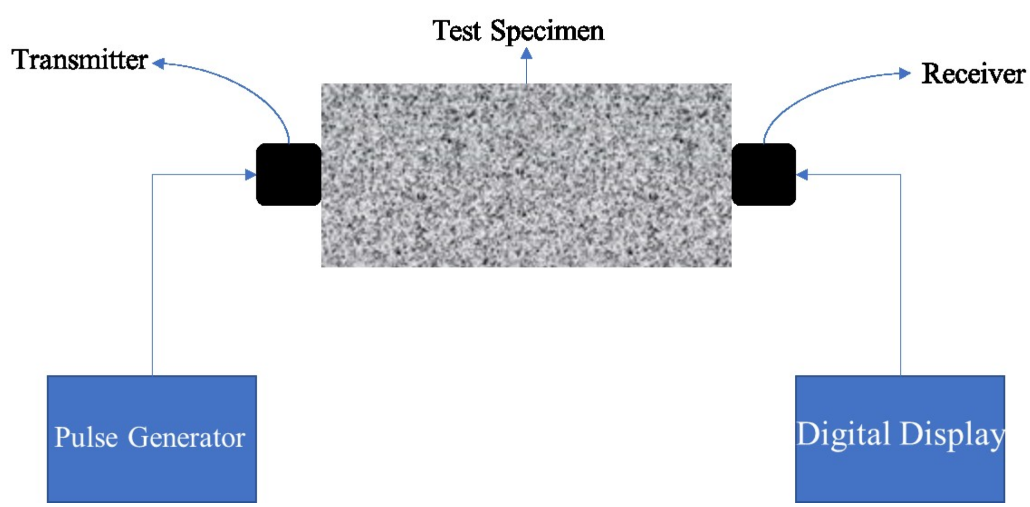

Figure 19: Ultrasonic Pulse Velocity (UPV) setup

The ultrasonic pulse velocity method continues to be improved through ongoing research. For example, some researchers have used the ultrasonic pulse velocity method to monitor the development of cracks in a concrete structure when under heating conditions, demonstrating the versatility of the method to evaluate structural integrity[169], [170]. The compressive strength of a concrete structure was also predicted through artificial neural networks using the densities and the velocity of waves traveling through the medium as input data [164], showing how the behavior of structures over time can be determined based on their ultrasonic pulse velocities.

The advantages of this method are that it has a simple evaluation procedure, it is easily deployed, and has a relatively low cost of use. One major drawback according to [165] is that there is a tendency for the S and P-waves to be indistinguishable in thin specimens.

1.7.1.5. Ultrasonic phased array method

The ultrasonic phased array method [170] uses multiple transducers for the purpose of scanning a surface using different configurations. Its use is codified in ASTM E2700 [171] A typical phased array system consists of multiple transducers [157], [170] that can be set up to all transmit at the same time then receive at the same time, to all transmit and receive at different times, or set so that some transmit while others are receiving simultaneously. The user usually has a bit of freedom in choosing the configuration of the phased array system to get specific results. A phased array system can be used to get many A-scans at once that are then interpreted using different algorithms, such as the 3D SAFT [172], to detect faults or even to check the health of a given structure. The basic phased array system is comprised of a set of transducers, a pulse generator, a receiver system, an amplifier, and typically a computer for signal processing.

The ultrasonic phased array method continues to be improved through ongoing research. For example, the phased array transducers have been reported to use flexible transducers that have the capability to stretch up to 50% to be able to access hard-to-reach surfaces for imaging purposes [173].

The advantages of this method are that it provides a means of improving the performance of low-frequency ultrasonic investigations and it can also be very useful because of its fast data acquisition. One major drawback is the possibility of having dead zones where the transmitter signals may be larger than the echo and thus suppress it, making it disadvantageous for very shallow flaws, like the case in [147] where the tendon ducts were not very visible.

1.7.1.6. Nonlinear ultrasonic method

The nonlinear ultrasonic method [174] measures the nonlinear response of solid structures from the excitation of linear ultrasonic sources. A strong nonlinear response typically occurs near deterioration of the structure or occurs due to microstructures that gives rise to nonlinear attenuation, amplitude-dependent phase delay [175] and resonance frequency shifts [176]. Typically, these are detected using Fourier analysis, which provides low amplitude signals below the noise level. Authors in [177], [178] propose a method called the scaling method to enhance the detection of such nonlinear ultrasonic properties.

The nonlinear ultrasonic method continues to be improved through ongoing research. For example, the scaling subtraction method [175] was introduced to replace the typical Fourier analysis of the nonlinear properties of the ultrasonic wave interaction [177] which is easier to implement and less dependent on the quality of the equipment used. [175].

The advantage of this method is that it provides a way of quantifying and detecting nonlinearity properties from the interaction of linear ultrasonic wave interaction with materials [177]. It can be used to monitor damage evolution [175]. In general, this can all be accomplished without a known baseline signal since the nonlinear components do not overlap with the excitation. One major drawback is that the method requires a high input signal amplitude, which requires a lot of power to generate [175].

1.7.1.7. Ultrasonic guided wave method

The ultrasonic guided wave method [179] utilizes a different approach from the bulk wave method where only a localized area under the probes is insonified [180] per time. This is the area that can be scanned at a time. The probes also need to be moved to cover the entire length. Ultrasonic guided waves on the other hand, use a single probe station [181] and a considerable length of a structure/device is scanned at once. The guided wave methods uses a transducer coupled to a wedge [181] to give an angle-beam excitation through a structure to insonify the structure and collect data from the interaction of the waves with the structure, where reflections from cracks and delaminations [179] can be seen and analyzed [180]. This method makes use of the sample sides for propagation because the waves are constantly bouncing back and forth in the structure creating overlaps between the waves and creating some form of interferences (constructive or destructive) [182]. A plot of the constructive interferences against the frequency exciting this gives a dispersion curve for the structure forming a wavenumber-frequency pair that shows what frequencies need to be excited to get certain velocities, hence, helping to design experiments that are specific for each structures as needed [149].

The advantage of this method is that it is inexpensive to implement since only a small amount of equipment is needed for implementation, saving cost on transducers and overall equipment size [183]. A major drawback is that the waves are dispersive meaning that the phase velocities are generally a factor of frequency [149] implying that each frequency used has a unique mode corresponding to it, hence limiting the use over a broader frequency band.

1.7.2. Sonic and ultrasonic nondestructive evaluation equipment

The most important sonic and ultrasonic nondestructive evaluation equipment are the transducers. The transducers perform the transmission and receiving in order to perform non-destructive testing.

1.7.2.1. Contact ultrasound transducers

Contact ultrasonic transducers are transmitters and receivers that send and receive ultrasonic waves to and from a structure when they are in contact with the surface of the element. They work by converting electrical signals into acoustic signals and vice versa through a device [149]. Contact ultrasound transducers usually require some form of couplant to reduce acoustical leakage into the areas surrounding the test structure, preventing a reduction in the efficiency of the transmission.

There are some advantages associated with the use of contact ultrasound transducers such as the ability to use them across most material types. For example, contact ultrasound is applicable to both reinforced and non-reinforced concrete structures. Yet, the downside is the need of a couplant to be able to use this transducer effectively.

1.7.2.2. Electromagnetic acoustic transducer (EMAT)

Electromagnetic acoustic transducers (EMAT) are electromagnetic devices to convert electrical energy to acoustic energy in the presence of a magnet [184]. It uses a coil that the electrical signal passes through that lies on a typically permanent magnet (sometimes electromagnets are used) to create a bias field that induces an acoustic signal in a conductive surface, which then transmits through the structure under test. The reverse happens at the receiving side, where the acoustic signal picked up from the structure is picked up and this induces an electric field in the coil in the presence of a magnetic field [185]

EMAT devices stand out due to a couple of facts. First, the devices do not require coupling to the surface being inspected. As a result, it is easier to use with rough surfaces and even curved surfaces. The second difference is that the magnetic component in the EMAT only enables it map out existing ferromagnetic parts of a structure. This makes the application of EMAT niche because it can only be used successfully with electrically conductive structures. Concrete structures with no metallic fibers or reinforcements may not be an applicable use for EMAT transducers. The use of EMAT transducers is codified in ASTM E1962 [186].

1.7.3. Radiography methods for concrete

An x-ray instrumentation system [187] employs electrically powered linear accelerators to generate x-rays, which are then beamed into the structure. This test is applied in a similar way to how medical x-rays are used to characterize bones and tissue. Soft x-rays, i.e. x-rays with lower frequencies and longer wavelengths (about 0.2 – 8 nm) [188] are used for medical practice [189]. In the case of inspecting structures, hard x-rays, x-rays with higher frequencies and shorter wavelengths (about 0.01 – 0.2 nm) , are used to better penetrate the structure [190]. As a result, protective measures are needed to prevent the exposure of humans to hard x-rays [191]. This is one reason why the x-ray method is most suited for enclosed spaces, where adequate protective measures can be put in place to ensure safety of the operator. There are lower-powered portable versions for use in the field [192].

While the x-ray method renders images in two-dimensions (2D), a computed tomography scan, or CT scan, is a three-dimensional (3D) scan [193] that uses x-ray radiation to determine the internal structure of materials, for example UHPC [194]. The CT scan method is very useful in determining the fiber orientation in the UHPC and as such is very useful for this UHPC project. One of the downsides to CT scanning however, is the fact that we can only scan a small sample at a time [194]–[196].

The gamma-ray method [197] can be the safer form of the x-ray method if the nuclear probe is carefully handled. The gamma-ray method uses a nuclear source with a probe that is in contact with or in a hole drilled into the structure under test. The gamma-ray method, however, requires more processing time than the X-ray method for the same size of structure [148].

1.7.4. Electrical methods for concrete NDE

The electrical impedance tomography method [198] tests the resistivity of concrete with electrodes that are spaced in a pattern, typically in a straight line according to the Wenner method as shown in Figure 20 [199]. The resistance between these electrodes is then measured. The electrodes must maintain good contact with the structure by drilling small holes into the structure. The resistivity method is usually good for testing electron mobility in the concrete, which is usually a measure of corrosion and chloride infiltration of the concrete structure or beam [148]. The main drawback is the need to maintain a good electrical contact with the structure at all times. This test method helps in determining the durability of concrete - even in the presence of reinforcement; there is research that has shown the resistivity values of UHPC are very low, and this method may be promising for use with UHPC for the Florida Department of Transportation (FDOT) [5], [200].

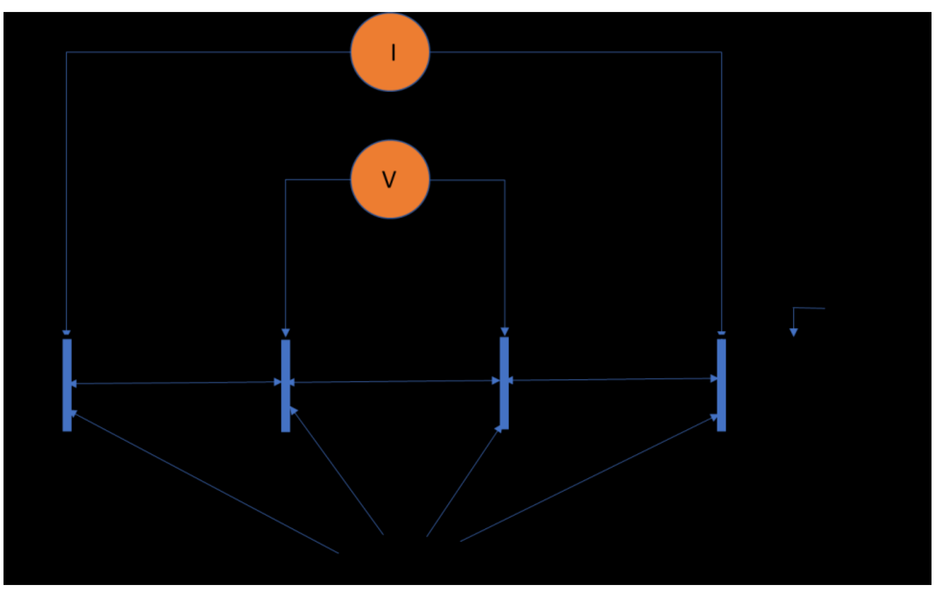

Figure 20: Wenner method

1.7.4.1. Half-cell potential measurement

Half-cell potential [148], [201] creates a contour map of concrete for detecting levels of corrosion damage. It typically entails comparing the potential of the steel reinforcement in a concrete structure to a reference half-cell electrode on the surface of the beam or structure. It is usually helpful in comparing regions that have been identified as having corrosion to those that are yet to be determined. A uniformly low potential typically indicates a corrosion risk. Also, a high potential gradient suggests localized corrosion [148]. It is standardized by ASTM C876 [202]. The main drawback is similar to that of the resistivity method in that you also need to drill a hole to make contact with the reinforced steel. It has been used to experimentally show that UHPC had lower corrosion probability when compared to some other concrete materials [203].

1.7.4.2. Galvanostatic pulse technique

The galvanostatic pulse technique is one of the oldest methods of corrosion testing in concrete reinforcement [204]. It was introduced for field application in response to the problems associated with the interpretation of corrosion risk assessment using the half-cell potential measurements of reinforcements. The method is a transient polarization method in the time-domain, where a short pulse is applied galvanostatically through a counter electrode to the concrete. This results in a change in the electrochemical potential of the steel reinforcement, which is recorded by a reference electrode that is typically situated at the center of the counter electrode. The ohmic resistance has to be evaluated based on the result received from the experiment. The corrosion level of the steel reinforcement can then be inferred from the calculation of the ohmic resistance of the steel reinforcement. This technique is codified as ASTM C876-91 [205].

1.7.5. Electromagnetic methods for concrete NDE

Electromagnetic methods have shown some promise for use in detecting steel fibers in concrete because of their magnetic properties. This test method is based on measuring the magnetic properties of steel fibers and is not applicable to polymer fibers.

1.7.5.1. Inductive Methods

Inductive methods have been shown to be useful for measuring the fiber content and orientation in test samples without macro-reinforcement [206], [207]. The steel fibers in UHPC give off a magnetic field. A coil wrapped around the concrete will pick up a difference in the magnetic field from the concrete in the form of an electrical signal. This inductance can be correlated with the volume of steel fibers in the concrete. Since steel fibers are long and slender, the magnetic field measured will be different depending on the direction of the fiber. By changing the axis about which the coil is wrapped around the sample, the orientation of the fibers can be measured to within 8.4 lb/yd^3 (5 kg/m^3) [206]. This method is often combined with the double punch test to determine sample strength and any contributions to the strength from fiber alignment. Application of this method to large structural members may be more difficult; however, as it would require a large coil, the ability to lift a structural member through the coil, the ability to change the axis of the structural member measured, and the ability to take into account any effects of reinforcing steel bars or steel prestressing strand.

1.7.5.2. Ground Penetrating Radar (GPR) Method/Impulse Radar Method

The ground penetrating radar method utilizes electromagnetic waves in the MHz to GHz region [208] from antennas to scan a concrete structure as shown in Figure 21. These waves are usually in the short-wavelength range, with frequencies ranging from 15 MHz to 3 GHz and can be tuned to achieve a desired resolution by selecting the right frequencies to use. For example, longer wavelengths are typically better for evaluating the insides of a masonry structure. The waves travel into the material, reflect and are then measured at the receiving antenna. The main difference between the GPR and the impulse radar method is that the impulse radar method typically uses higher frequencies than the GPR [147], whereas GPR uses lower frequencies compared to the impulse radar. The main drawback of this method is the high rate of absorption by the medium, making it difficult to achieve high resolution and excellent depth penetration simultaneously [209]. The method is useful for the evaluation of masonry arch bridges and harbor dock walls [148] and can be used to inspect structures that are built using UHPC.

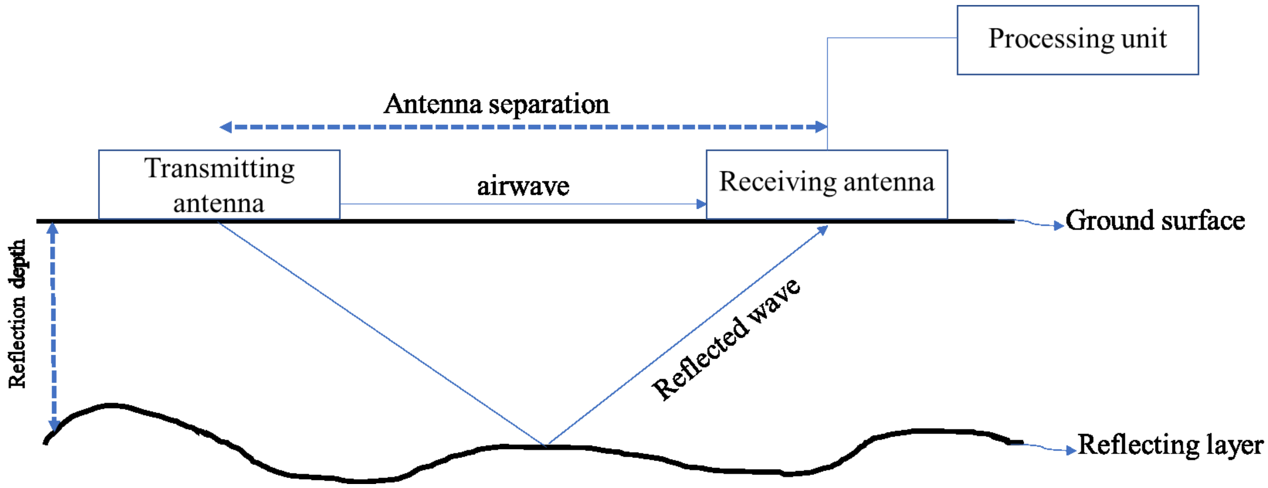

Figure 21: Ground Penetrating Radar

1.7.5.3. Cover Meter

A cover meter [148] is used to determine the location of steel rebar and the thickness of the concrete covering the rebar, as shown in Figure 22. The meter consists of two coils that are placed on an iron-cored inductor, and current is passed through one coil, which in turn induces a current in the second coil that is amplified and measured [148]. The magnitude of the induced current in the second coil is determined by the size of the steel bars and the thickness of the concrete cover. This is a good approach for measuring how thick concrete covering a reinforcement is because the magnitude of the induced current is influenced by the thickness of the concrete cover. With some adaption, there may be the possibility of adapting this technology to steel fiber detection in UHPC.

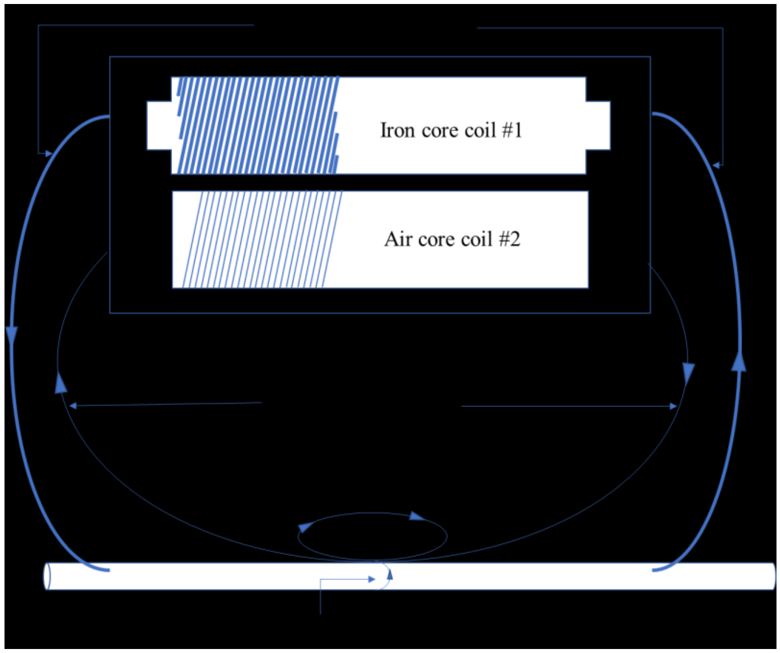

Figure 22: Cover meter basic operation

1.7.6. Thermography methods for concrete NDE

Infrared thermography [210] is a method that measures heat from infrared rays emitted by the concrete surface with specialized cameras. These signals are converted into a temperature map and a color scale indicates the relative temperature differences of that surface. For concrete structures, an even surface and homogeneous thickness produce a uniform temperature signature. In contrast, structures tend to heat up faster in those regions that have delaminations or other defects, creating a difference from the homogeneous regions [148] . This is a very good diagnostic method for large structures where the heatmap can be easily observed and the regions with defects can be monitored and inspected further.

1.8. Summary

UHPC has many unique properties that make it an excellent candidate material to make structural members that are stronger, longer, and more durable than those under current practices. In order to use UHPC, quality control test methods are needed to measure its true properties and ensure that it has the expected durability and tensile strength everywhere desired. A review of potential test methods for plant quality control use was performed, showing that many test methods exist, and that with some adaption may be used for UHPC.

1.9. References

[1] J. Dils, V. Boel, and G. De Schutter, "Influence of cement type and mixing pressure on air content , rheology and mechanical properties of UHPC," *Constr. Build. Mater.*, vol. 41, pp. 455–463, 2013.

[2] E. M. Williams *et al.*, "Laboratory Characterization of Cor-Tuf Concrete With and Without Steel Fibers," *Tech. Rep. No. ERDC/GSL TR-02-22, U.S. Army Corps Eng. Eng. Res. Dev. Center, Washington, DC*, no. 7, pp. 1–74, 2009.

[3] T. Nuruddin, M. F., Khan, S. U., Shafiq, N., & Ayub, "Strength Development of High-Strength Ductile Concrete Incorporating Metakaolin and PVA Fibers," *Sci. World J.*, pp. 1–11, 2014.

[4] R. Haber, Z. B., De la Varga, I., Graybeal, B. A., Nakashoji, B., & El-Helou, "Properties and Behavior of UHPC-Class Materials," *(No. FHWA-HRT-18-036). United States. Fed. Highw. Adm. Off. Infrastruct. Res. Dev.*, no. 3, pp. 1–153, 2018.

[5] W. Meng, M. Valipour, and K. H. Khayat, "Optimization and performance of cost-effective ultra-high performance concrete," *Mater. Struct. Constr.*, vol. 50, no. 1, pp. 1–16, Feb. 2017.

[6] K. H. Meng, W., & Khayat, "Effect of Hybrid Fibers on Fresh Properties , Mechanical Properties , and Autogenous Shrinkage of Cost-Effective UHPC," *J. Mater. Civ. Eng.*, vol. 30, no. 4, pp. 1–8, 2018.

[7] K. Wille, D. Joo, and K. Antoine, "Strain-hardening UHP-FRC with low fiber contents," *Mater. Struct.*, vol. 44, no. 3, pp. 583–598, 2011.

[8] S. H. Park, D. J. Kima, G. S. Ryub, and K. T. Koh, "Tensile behavior of Ultra High Performance Hybrid Fiber Reinforced Concrete," *Cem. Concr. Compos.*, vol. 34, no. 2, pp. 172–184, 2012.

[9] Q. Song, R. Yu, X. Wang, S. Rao, and Z. Shui, "A novel Self-Compacting Ultra-High Performance Fibre Reinforced Concrete (SCUHPFRC) derived from compounded high-active powders," *Constr. Build. Mater.*, vol. 158, pp. 883–893, 2018.

[10] M. Alkaysi and S. El-Tawil, "Structural Response of Joints Made with Generic UHPC," *Struct. Congr.*, pp. 1435–1445, 2015.

[11] H. G. Russell and Benjamin A. Graybeal, "Ultra-High Performance Concrete : A State-of-the-Art Report for the Bridge Community," *(No. FHWA-HRT-13-060). United States. Fed. Highw. Adm. Off. Infrastruct. Res. Dev.*, pp. 1–163, 2013.

[12] L. Felipe, M. Duque, and B. A. Graybeal, "Fiber Reinforcement Influence on the Tensile Response of UHPFRC," *First Int. Interact. Symp. UHPC-2016 (Des Moines, IOWA, Jul. 18–20).*, pp. 1–10, 2016.

[13] W. Meng and K. H. Khayat, “Improving flexural performance of ultra-high-performance concrete by rheology control of suspending mortar Improving fl exural performance of ultra-high-performance concrete by rheology control of suspending mortar,” *Compos. Part B*, vol. 117, no. 2, pp. 26–34, 2017.

[14] L. Ferrara, M. Prisco, and M. G. L. Lamperti, “Identification of the stress-crack opening behavior of HPFRCC : the role of flow-induced fiber orientation,” *Proc. Fram.*, vol. 7, pp. 1541–1550, 2010.

[15] P. Sta and J. G. M. Van Mier, “Manufacturing , fibre anisotropy and fracture of hybrid fibre concrete,” *Eng. Fract. Mech.*, vol. 74, no. 1–2, pp. 223–242, 2007.

[16] K. H. Khayat, W. Meng, K. Vallurupalli, and L. Teng, “Rheological properties of ultra-high-performance concrete -An overview,” *Cem. Concr. Res.*, vol. 124, pp. 1–16, 2019.

[17] H. G. Russell and B. A. Graybeal, “Ultra-High Performance Concrete : A State-of-the-Art Report for the Bridge Community,” *(No. FHWA-HRT-13-060). United States. Fed. Highw. Adm. Off. Infrastruct. Res. Dev.*, no. 6, 171 pp.,2013.

[18] CSA 23.3, “Design of Concrete Structures - Draft.” Canadian Standards Association, 2018.

[19] D. Yoo, G. Zi, S. Kang, and Y. Yoon, “Biaxial flexural behavior of ultra-high-performance fi ber-reinforced concrete with different fi ber lengths and placement methods,” *Cem. Concr. Compos.*, vol. 63, no. 7, pp. 51–66, 2015.

[20] L. Felipe, M. Duque, and B. Graybeal, “Fiber orientation distribution and tensile mechanical response in UHPFRC,” *Mater. Struct.*, vol. 50, no. 1, pp. 1–17, 2017.

[21] ASTM C1609, “Standard Test Method for Flexural Performance of Fiber-Reinforced Concrete (Using Beam With Third-Point Loading) 1,” *West Conshohocken, PA; ASTM Int.*, pp. 1–9, 2012.

[22] K. Wille and G. J. Parra-montesinos, “Effect of Beam Size, Casting Method, and Support Conditions on Flexural Behavior of Ultra-High-Performance Fiber-Reinforced Concrete,” *ACI Mater. J.*, vol. 109, no. 3, pp. 379–388, 2013.

[23] H. Huang, X. Gao, L. Li, and H. Wang, “Improvement effect of steel fiber orientation control on mechanical performance of UHPC,” *Constr. Build. Mater.*, vol. 188, no. 8, pp. 709–721, 2018.

[24] D. Yoo, S. Kang, and Y. Yoon, “Effect of fiber length and placement method on flexural behavior, tension-softening curve, and fiber distribution characteristics of UHPFRC,” *Constr. Build. Mater.*, vol. 64, no. 4, pp. 67–81, 2014.

[25] M. Roy, C. Hollmann, and K. Wille, “Influence of volume fraction and orientation of fibers on the pullout behavior of reinforcement bar embedded in ultra high performance concrete,” *Constr. Build. Mater.*, vol. 146, no. 4, pp. 582–593, 2017.

[26] J. Park, Y. J. Kim, J. Cho, and S. Jeon, "Early-Age Strength of Ultra-High Performance Concrete in Various Curing Conditions," *Materials (Basel).*, vol. 8, no. 8, pp. 5537–5553, 2015.

[27] K.-T. Koh, J.-J. Park, G.-S. Ryu, and S.-T. Kang, "Effect of the compressive strength of ultra-high strength steel fiber reinforced cementitious composites on curing method," *J. Korean Soc. Civ. Eng.*, vol. 27, no. 3, pp. 427–432, 2007.

[28] H. Yazıcı, M. Y. Yardımcı, S. Aydın, and S. Anıl, "Mechanical properties of reactive powder concrete containing mineral admixtures under different curing regimes," *Constr. Build. Mater.*, vol. 23, no. 3, pp. 1223–1231, 2009.

[29] A. . & Vigneshwari.M, "Experimental investigation on ultra high strength concrete containing mineral admixtures under different curing conditions," *Int. J. Civ. Struct. Eng.*, vol. 2, no. 1, pp. 33–42, 2011.

[30] Q. Gu, C., Sun, W., Guo, L., & Wang, "Effect of Curing Conditions on the Durability of Ultra- high Performance Concrete under Flexural Load," *J. Wuhan Univ. Technol. Sci. Ed.*, vol. 31, no. 2, pp. 278–285, 2016.

[31] D. Wang, C. Shi, Z. Wu, J. Xiao, Z. Huang, and Z. Fang, "A review on ultra high performance concrete : Part II . Hydration , microstructure and properties," *Constr. Build. Mater.*, vol. 96, no. 8, pp. 368–377, 2015.

[32] M. Richard, P.; Cheyrezy, "Composition of reactive powder concretes," *Cem. Concr. Res.*, vol. 25, no. 7, pp. 1501–1511, 1995.

[33] U. Mueller, P. Fontana, and C. Lehmann, "Effects of Autoclaving on the Nano structure and Phase composition of Ultra High Performance Concrete," *12th Euroseminar Microsc. Appl. to Build. Mater.*, pp. 1–9, 2009.

[34] M. Cheyrezy, V. Maret, and L. Frouin, "Microstructural Anaylsis of RPC (Reactive Powder Concrete)," *Cem. Concr. Res.*, vol. 25, no. 7, pp. 1491–1500, 1995.

[35] O. H. Wallevik and J. E. Wallevik, "Rheology as a tool in concrete science: The use of rheographs and workability boxes," *Cem. Concr. Res.*, vol. 41, no. 12, pp. 1279–1288, 2011.

[36] K. Hsu, J. Chiu, S. Chen, and Y. Tseng, "Effect of addition time of a superplasticizer on cement adsorption and on concrete workability," *Cem. Concr. Compos.*, vol. 21, no. 5–6, pp. 425–430, 1999.

[37] J. Plank, C. Schröfl, and M. Gruber, "Use of a Supplemental Agent to Improve Flowability of Ultra-High- Performance Concrete," *Ninth ACI Intern. Conf. on Superplasticizers and Other Chem. Admix.*, No. SP-262, Ed. Gupta, P., Holland, T.C., and Malhotra, V.M., 2009, pp. 1-16.

[38] D. Wang, C. Shi, Z. Wu, J. Xiao, Z. Huang, and Z. Fang, "A review on ultra high

performance concrete : Part II . Hydration , microstructure and properties," *Constr. Build. Mater.*, vol. 96, no. 8, pp. 368–377, 2015.

[39] M. Courtial, M. De Noirfontaine, F. Dunstetter, M. Signes-frehel, and P. Mounanga, "Effect of polycarboxylate and crushed quartz in UHPC : Microstructural investigation," *Constr. Build. Mater.*, vol. 44, no. 8, pp. 699–705, 2013.

[40] K. Wille, A. E. Naaman, and G. J. Parra-montesinos, "Ultra-High Performance Concrete with Compressive Strength Exceeding 150 MPa (22 ksi): A Simpler Way," *ACI Mater. J.*, vol. 108, no. 1, pp. 46–54, 2011.

[41] P. Feylessoufi, A., Crespin, M., Dion, P., Bergaya, F., Van Damme, H., & Richard, "Controlled Rate Thermal Treatment of Reactive Powder Concretes," *Elsevier Sci. Ltd*, vol. 6, no. 1, pp. 1501–1511, 1997.

[42] F. Hirschi, T., & Wombacher, "Influence of different superplasticizers on UHPC," *Proc. Second Int. Symp. Ultra High Perform. Concr. Kassel Univ. Press. Kassel*, pp. 77–84, 2008.

[43] A. Yahia and M. Tanimura, "Rheology of belite-cement - Effect of w/c and high-range water-reducer type," *Constr. Build. Mater.*, vol. 88, no. 4, pp. 169–174, 2015.

[44] ASTM C1856, "Standard Practice for Fabricating and Testing Specimens of Ultra-High," *West Conshohocken, PA; ASTM Int.*, pp. 1–4, 2017.

[45] ASTM C1437, "Standard Test Method for Flow of Hydraulic Cement Mortar," *West Conshohocken, PA; ASTM Int.*, pp. 1–2, 2015.

[46] ASTM C1856, "Standard Practice for Fabricating and Testing Specimens of Ultra-High Performance Concrete," *West Conshohocken, PA; ASTM Int.*, pp. 1–4, 2017.

[47] N. Roussel, C. Stefani, and R. Leroy, "From mini-cone test to Abrams cone test : measurement of cement-based materials yield stress using slump tests," *Cem. Concr. Res.*, vol. 35, no. 5, pp. 817–822, 2005.

[48] S. P. Tregger, N., Ferrara, L., & Shah, "Identifying viscosity of cement paste from mini-slump-flow test," *ACI Mater. J.*, vol. 105, no. 6, p. 558, 2008.

[49] M. Sung, J. Soo, K. Seong, K. Koh, and S. Hee, "Estimation of rheological properties of UHPC using mini slump test," *Constr. Build. Mater.*, vol. 106, no. 1, pp. 632–639, 2016.

[50] K. A. Riding, C. C. Ferraro, H. R. Hamilton, M. S. Voss, and R. S. Alrashidi, "Requirements for Use of Field-Cast, Proprietary Ultra-High-Performance Concrete in Florida Structural Applications Final report," *Univ. Florida, Draft Tech. Memo. BDV-31 TWO 977-94*, no. 4, pp. 1–195, 2019.

[51] J. P. Binard, "UHPC: A Game-Changing Material for PCI Bridge Producers," *PCI J.*, vol. 62, no. 2, pp. 34–46, 2017.

[52] H. Lee, H. Jang, and K. Cho, “Evaluation of Bonding Shear Performance of Ultra-High-Performance Concrete with Increase in Delay in Formation of Cold Joints,” *Materials (Basel).*, vol. 9, no. 5, pp. 1–15, 2016.

[53] C. K. Crane and L. F. Kahn, “Interface Shear Capacity of Small UHPC / HPC Composite T-Beams,” *Ultra-High Perform. Concr. Nanotechnol. Constr. Proc. Hipermat 2012. 3rd Int. Symp. UHPC Nanotechnol. High Perform. Constr. Mater.*, no. 19, pp. 495–467, 2012.

[54] ASTM C403, “Standard Test Method for Time of Setting of Concrete Mixtures by Penetration Resistance,” *West Conshohocken, PA; ASTM Int.*, pp. 1–7, 2016.

[55] ASTM C191, “Standard Test Methods for Time of Setting of Hydraulic Cement by Vicat Needle,” *West Conshohocken, PA; ASTM Int.*, pp. 1–8, 2019.

[56] R. Li, P., Yu, Q., Brouwers, H. J. H., & Yu, “Fresh behaviour of ultra-high performance concrete (UHPC) : an investigation of the effect of superplasticizers and steel fibres,” *Proc. 9th Int. Concr. Conf. 2016, Environ. Effic. Econ. Challenges Concr. Dundee, Scotland, United Kingdom*, pp. 635–644, 2016.

[57] D. B. Valentim, S. Aaleti, A. Amirkhanian, and M. E. Kreger, “Experimental Evaluation of Test Methods to Characterize Tensile Behavior of Ultra-High Performance Concrete,” in *Second International Interactive Symposium on UHPC*, 2019, pp. 1–10.

[58] C. Molins, A. Aguado, and S. Saludes, “Double punch test to control the energy dissipation in tension of FRC (Barcelona test),” *Mater. Struct. Constr.*, vol. 42, no. 4, pp. 415–425, 2009.

[59] ASTM C1018, “Standard Test Method for Flexural Toughness and First-Crack Strength of Fiber-Reinforced Concrete (Using Beam With Third-Point Loading) 1,” *West Conshohocken, PA; ASTM Int.*, pp. 1–8, 1997.

[60] B. A. Graybeal and F. Baby, “Tension Testing of Ultra-High Performance Concrete,” *(No. FHWA-HRT-17-053). United States. Fed. Highw. Adm. Off. Infrastruct. Res. Dev.*, pp. 1–186, 2019.

[61] F. Baby, B. Graybeal, P. Marchand, and F. Toutlemonde, “Proposed Flexural Test Method and Associated Inverse Analysis for Ultra-High-Performance Fiber-Reinforced Concrete,” *ACI Mater. J.*, vol. 109, no. 5, pp. 545–556, 2012.

[62] ASTM C496, “Standard Test Method for Splitting Tensile Strength of Cylindrical Concrete Specimens,” *West Conshohocken, PA; ASTM Int.*, pp. 1–5, 2017.

[63] B. A. Graybeal, “Practical Means for Determination of the Tensile Behavior of Ultra-High Performance Concrete,” *J. ASTM Int.*, vol. 3, no. 8, pp. 1–9, 2006.

[64] H. A. Goaiz, T. Yu, and M. N. S. Hadi, *Quality evaluation tests for tensile strength of reactive powder concrete*, vol. 30, no. 5. 2018.

[65] C. Ozyildirim, "Evaluation of Ultra-High-Performance Fiber-Reinforced Concrete," *(No. FHWA/VCTIR 12-R1). Virginia Cent. Transp. Innov. Res.*, pp. 1–20, 2011.

[66] M. Prisco, M. G. L. Lamperti, and S. Lapolla, "Double-edge wedge splitting test: preliminary results," *Fract. Mech. Concr. Concr. Struct.*, pp. 1579–1586, 2010.

[67] UNE 83515, "Fiber Reinforced Concrete. Determination of Cracking Strength, Ductility and Residual Tensile Strength. Barcelona Test." Asociacion Espanola de Normalizacion y Certifiación, pp. 1–10, 2010.

[68] W. F. Chen and T. Colgrove, "DOUBLE-PUNCH TEST FOR TENSILE STRENGTH OF CONCRETE," *Transp. Res. Rec. J. Transp. Res. Board*, vol. 504, pp. 43–50, 1974.

[69] S. Tuladhar, "A standard tensile testing procedure for fiber-reinforced concrete (FRC) and UHPFRC based on double punch test(DPT)," *Master thesis, Univ. Texas Arlingt.*, December, pp. 1–189, 2017.

[70] P. Pujadas, A. Blanco, S. Cavalaro, A. de la Fuente, and A. Aguado, "New Analytical Model To Generalize The Barcelona Test Using Axial Displacement," *J. Civ. Eng. Manag.*, vol. 19, no. 2, pp. 259–271, Apr. 2013.

[71] E. Galeote, A. Blanco, S. H. P. Cavalaro, and A. de la Fuente, "Correlation between the Barcelona test and the bending test in fibre reinforced concrete," *Constr. Build. Mater.*, vol. 152, pp. 529–538, Oct. 2017.

[72] D. Choumanidis, E. Badogiannis, P. Nomikos, and A. Sofianos, "Barcelona test for the evaluation of the mechanical properties of single and hybrid FRC, exposed to elevated temperature," *Constr. Build. Mater.*, vol. 138, no. 5, pp. 296–305, May 2017.

[73] S. H. Chao, N. B. Karki, J. S. Cho, and R. N. Waweru, "Use of double punch test to evaluate the mechanical performance of fiber reinforced concrete," in *Proceedings of the 6th International Workshop on High Performance Fiber Reinforced Cement Composites (HPFRCC6)*, 2011, pp. 27–34.

[74] K. Wille, S. El-tawil, and A. E. Naaman, "Properties of strain hardening ultra high performance fiber reinforced concrete (UHP-FRC) under direct tensile loading," *Cem. Concr. Compos.*, vol. 48, no. 1, pp. 53–66, 2014.

[75] B. A. Graybeal and F. Baby, "Development of direct tension test method for ultra-high-performance fiber-reinforced concrete," *ACI Mater. J.*, vol. 110, no. 2, pp. 177–186, 2013.

[76] ASTM C39, "Standard Test Method for Compressive Strength of Cylindrical Concrete Specimens," *West Conshohocken, PA; ASTM International*. ASTM International, pp. 1–7, 2018.

[77] N. Roux, C. Andrade, and M. A. Sanjuan, "Experimental Study of Durability of Reactive Powder Concretes," *J. Mater. Civ. Eng.*, vol. 8, no. February, pp. 1–6, 1996.

[78] O. Bonneau, C. Vernet, M. Moranville, and P. Aitcin, "Characterization of the granular packing and percolation threshold of reactive powder concrete," *Cem. Concr. Res.*, vol. 30, no. 12, pp. 1861–1867, 2000.

[79] C. Vernet, "UHPC microstructure and related durability perfor-mance laboratory assessment and field experience examples," in *Proceedings of 2003 International Symposium on High Performance Concrete*, 2003.

[80] T. Ahlborn, D. K. Harris, D. L. Misson, and E. J. Peuse, "Durability and Strength Characterization of Ultra-High Performance Concrete Under Variable Curing Regimes," in *Ultra High Performance Concrete: Proceedings of the Second International Symposium on Ultra High Performance Concrete*, 2008, pp. 197–204.

[81] M. Acker, P., & Behloul, "Ductal® technology: A large spectrum of properties, a wide range of applications," *Proc. Int. Symp. UHPC Kassel, Ger.*, pp. 11–23, 2004.

[82] J. Piérard, B. Dooms, and N. Cauberg, "Durability Evaluation of Different Types of UHPC," *Proc. RILEM-fib-AFGC Int. Symp. Ultra-High Perform. Fibre-Reinforced Concr.*, pp. 275–284, 2013.

[83] M. Lee, K. Lee, and M. Tia, "UHPC Precast Product under Severe Freeze-Thaw Conditions," *In ICF13*, pp. 1–8, 2013.

[84] Z. Zhou, "Development, Characterization and Modeling of Ultra-high Performance Concrete (UHPC) with Locally Available Materials," *Dr. Diss. Washingt. State Univ.*, pp. 1–219, 2018.

[85] C. P.Vernet, "Ultra-Durable Concretes : Structure at the Micro- and Nanoscale," *MRS Bull.*, vol. 29, no. 5, pp. 324–327, 2004.

[86] M. Thomas, B. Green, E. O'Neal, V. Perry, S. Hayman, and A. Hossack, "Marine performance of UHPC at Treat Island," in *Proceedings of Hipermat 2012 3rd International Symposium on UHPC and Nanotechnology for High Performance Construction Materials*, 2012, pp. 365–370.

[87] J. J. Valenza and G. W. Scherer, "Mechanism for Salt Scaling," *J. Am. Ceram. Soc.*, vol. 89, no. 4, pp. 1161–1179, 2006.

[88] B. A. Graybeal, "Material Property Characterization of Ultra-High Performance Concrete," *(No. FHWA-HRT-06-103). United States. Fed. Highw. Adm. Off. Infrastruct. Res. Dev.*, pp. 1–176, 2006.

[89] M. Schmidt, E. Fehling, T. Teichmann, and K. Bunje, "Durability of Ultra High Performance Concrete," in *Proceedings of the 6th International Symposium on High Strength/High Performance Concrete*, 2002, pp. 1367–1376.

[90] S. El-tawil, M. Alkaysi, A. E. Naaman, W. Hansen, and Z. Liu, "Development, Characterization and Applications of a Non Proprietary Ultra High Performance Concrete

for Highway Bridges," *Michigan. Dept. Transp.*, pp. 1–42, 2016.

[91] Z. Li, K. Afshinnia, and P. R. Rangaraju, "Effect of alkali content of cement on properties of high performance cementitious mortar," *Constr. Build. Mater.*, vol. 102, no. 11, pp. 631–639, 2016.

[92] ASTM C1567, "Standard Test Method for Determining the Potential Alkali-Silica Reactivity of Combinations of Cementitious Materials and Aggregate (Accelerated Mortar-Bar Method)," *West Conshohocken, PA; ASTM Int.*, pp. 1–6, 2013.

[93] B. Möser, C. Pfeifer, and J. Stark, "Durability and microstructural development during hydration in ultra-high performance concrete," *Taylor Fr. Group, London*, pp. 87–88, 2009.

[94] Y. L. M. and M. L. Jamshaid Sawab, Ing Lim, "Ultra-High-Performance Concrete And Advanced Manufacturing Methods For Modular Construction," *(No. FY-ID-13-5282 CA-13-TX-UH-0606-0122). Univ. Houston, Houston, TX (United States).*, pp. 1–284, 2016.

[95] J. Pitroda and F. S. Umrigar, "Evaluation of Sorptivity and Water Absorption of Concrete with Partial Replacement of Cement by Thermal Industry Waste (Fly Ash)," *Int. J. Eng. Innov. Technol.*, vol. 2, no. 7, pp. 245–249, 2013.

[96] K. A. Snyder, "The relationship between the formation factor and the diffusion coefficient of porous materials saturated with concentrated electrolytes: Theoretical and experimental considerations," *Concr. Sci. Eng.*, vol. 3, no. 12, pp. 216–224, 2001.

[97] G. E. Archie, "The Electrical Resistivity Log as an Aid in Determining Some Reservoir Characteristics," *Trans. AIME*, vol. 146, no. 1, pp. 54–62, 1942.

[98] R. Spragg, Y. Bu, K. Snyder, D. Bentz, and J. Weiss, "Electrical Testing of Cement-Based Materials: Role of Testing Techniques, Sample Conditioning," *Publ. FHWA/IN/JTRP-2013/28. Jt. Transp. Res. Program, Indiana Dep. Transp. Purdue Univ. West Lafayette, Indiana*, pp. 1–20, 2013.

[99] Y. Bu and J. Weiss, "The influence of alkali content on the electrical resistivity and transport properties of cementitious materials," *Cem. Concr. Compos.*, vol. 51, no. 3, pp. 49–58, 2014.

[100] R. Spragg, L. Montanari, I. Varga, and B. A. Graybeal, "Using Formation Factor to Define the Durability of Ultra-High Performance Concrete," *Second International Interactive Symposium on Ultra High Performance Concrete*, pp. 1–11, 2019.

[101] AASHTO T 358, "Standard Method of Test for Surface Resistivity Indication of Concrete's Ability to Resist Chloride Ion Penetration.," *AASHTO Provisional Stand.* pp. 1–8, 2015.

[102] Proceq SA, "The world's most accurate concrete surface resistivity meter," pp. 1-4, 2016. https://www.proceq.com/uploads/tx_proceqproductcms/import_data/files/Resipod_Sales%20Fl

yer_English_high.pdf

[103] AASHTO TP 119, "Standard Method of Test for Electrical Resistivity of a Concrete Cylinder Tested in a Uniaxial Resistance Test," *Am. Assoc. State Highw. Transp. Off.*, pp. 1–11, 2015.

[104] ASTM C1202, "Standard Test Method for Electrical Indication of Concrete's Ability to Resist Chloride," *West Conshohocken, PA; ASTM Int.*, pp. 1–8, 2019.

[105] ASTM C1202, "Standard Test Method for Electrical Indication of Concrete's Ability to Resist Chloride Ion Penetration," *Am. Soc. Test. Mater.*, pp. 1–8, 2012.

[106] J. D. Shane, C. D. Aldea, N. F. Bouxsein, T. O. Mason, H. M. Jennings, and S. P. Shah, "Microstructural and pore solution changes induced by the rapid chloride permeability test measured by impedance spectroscopy," *Concr. Sci. Eng.*, vol. 1, no. 2, pp. 110–119, 1999.

[107] K. A. Riding, J. L. Poole, A. K. Schindler, M. C. G. Juenger, and K. J. Folliard, "Simplified concrete resistivity and rapid chloride permeability test method," *ACI Mater. J.*, vol. 105, no. 4, pp. 390–394, 2008.

[108] Z. Li, "Proportioning And Properties Of Ultra-High Performance Concrete Mixtures For Application In Shear Keys Of Precast Concrete Bridges," *Diss.*, Clemson Univ., 339 pp., 2015.

[109] NT Build 492, "Concrete, mortar and cement-based repair materials: Chloride migration coefficient from non-steady-state migration experiments," *Nord. method*, pp. 1–8, 1999.

[110] J. P. Vincler, T. Sanchez, V. Turgeon, D. Conciatori, and L. Sorelli, "A modified accelerated chloride migration tests for UHPC and UHPFRC with PVA and steel fibers," *Cem. Concr. Res.*, vol. 117, no. 12, pp. 38–44, 2018.

[111] S. H. G. Mosavinejad, M. Alimohammad, J. Barandoust, and A. Ghanizadeh, "Electrical and microstructural analysis of UHPC containing short PVA fibers," *Constr. Build. Mater.*, vol. 235, no. 11, pp. 1–17, 2019.

[112] A. Rafiee, "Computer Modeling and Investigation on the Steel Corrosion in Cracked Ultra High Performance Concrete," *Kassel Univ. Press GmbH.*, no. 21, p. 219, 2012.

[113] M. Jooss and H. W. Reinhardt, "Permeability and diffusivity of concrete as function of temperature," *Cem. Concr. Res.*, vol. 32, no. 9, pp. 1497–1504, 2002.

[114] ASTM C1556, "Standard Test Method for Determining the Apparent Chloride Diffusion Coefficient of Cementitious Mixtures by Bulk Diffusion," *West Conshohocken, PA; ASTM Int.*, pp. 1–7, 2016.

[115] ASTM C1152, "Standard Test Method for Acid-Soluble Chloride in Mortar and Concrete," *West Conshohocken, PA; ASTM Int.*, pp. 1–4, 2012.

[116] J. Piérard, B. Dooms, and N. Cauberg, "Evaluation of Durability Parameters of UHPC Using Accelerated Lab Tests," *Proc. 3rd Int. Symp. UHPC Nanotechnol. High Perform. Constr. Mater. Kassel, Ger.*, pp. 371–376, 2012.

[117] M. A. Roux, N., Andrade, C., & Sanjuan, "Experimental Study Of Durability Of Reactive Powder Concretes," *J. Mater. Civ. Eng.*, vol. 8, no. 1, pp. 1–6, 1996.

[118] ASTM C1585, "Standard Test Method for Measurement of Rate of Absorption of Water by Hydraulic Cement Concretes," *ASTM Int.*, pp. 4–9, 2013.

[119] BS EN 12390-8, "Testing hardened concrete. Depth of penetration of water under pressure," 2009.

[120] J. Castro, D. Bentz, and J. Weiss, "Effect of sample conditioning on the water absorption of concrete," *Cem. Concr. Compos.*, vol. 33, no. 8, pp. 805–813, 2011.

[121] S. Zhutovsky and R. D. Hooton, "Role of sample conditioning in water absorption tests," *Constr. Build. Mater. J.*, vol. 215, no. 5, pp. 918–924, 2019.

[122] E. Ghafari, H. Costa, E. Júlio, and A. Portugal, "Enhanced Durability of Ultra High Performance Concrete by Incorporating Supplementary Cementitious Materials," *2nd Int. Conf. microdurability Delft, Netherl.*, no. 4, pp. 86–94, 2012.

[123] E. F. O'Neil, C. E. Dauriac, and S. K. Gililand, "Development of Reactive Powder Concrete (RPC) Products in the United States Construction Market," *High- Strength Concr. An Int. Perspect. Pap. Present. three halfday Sess. ACI Conv. Montr. SP-167*, pp. 249–261, 1997.

[124] P. Rougeau, B. Borys, "Ultra High Performance Concrete with ultrafine particles other than silica fume," *Proc. Int. Symp. ultra High Perform. Concr. Kassel, Ger. Univ. Kassel, Ger.*, pp. 213-224, 2004.

[125] P. Smarzewski and D. Barnat-hunek, "Effect of Fiber Hybridization on Durability Related Properties of Ultra-High Performance Concrete," *Int. J. Concr. Struct. Mater.*, vol. 11, no. 2, pp. 315–325, 2017.

[126] H. Giesche, "Mercury Porosimetry : A General (Practical) Overview," *Particle & particle systems characterization.,* vol. 23, no. 9, pp. 9–19, 2006.

[127] K. Tanaka and K. Kurumisawa, "Development of technique for observing pores in hardened cement paste," *Cem. Concr. Res.*, vol. 32, no. 9, pp. 1435–1441, 2002.

[128] D. A. Abell, A. B., Willis, K. L., & Lange, "Mercury Intrusion Porosimetry and Image Analysis of Cement-Based Materials," *J. Colloid Interface Sci.*, vol. 211, no. 1, pp. 39–44, 1999.

[129] R. A. Cook and K. C. Hover, "Mercury porosimetry of hardened cement pastes," *Cem. Concr. Res.*, vol. 29, no. 6, pp. 933–943, 1999.

[130] Sung-Hoon Kang, J.-H. Lee, S.-G. Hong, and J. Moon, “Microstructural Investigation of Heat-Treated Ultra-High Performance Concrete for Optimum Production,” *Materials (Basel).*, vol. 10, no. 9, pp. 1–13, 2017.

[131] M. Zhang and H. Li, “Pore structure and chloride permeability of concrete containing nano-particles for pavement,” *Constr. Build. Mater.*, vol. 25, no. 2, pp. 608–616, 2011.

[132] D. Daniel, M. Kouril, N. Radka, P. Petr, and P. Radka, “Measurement of Chloride Permeability in UHPC by Accelerated Method,” *Solid State Phenom.*, vol. 259, no. 2, pp. 80–84, 2017.

[133] & S. M. Roux N., Andrade C., “Experimental study of Durability of Reactive Powder Concrete,” *Journal of Mater in Civil Eng.,* vol. 8, no. 2, pp. 1–6, 1996.

[134] J. Andrade, C., & Torres, “Long Term Carbonation of UHPC,” *Proc. Int. Symp. Ultra-High Perform. Fiber-Reinforced Concr. Marseille, Fr.*, vol. 4, no. 1, pp. 249–256, 2013.

[135] ACI 201.2, “Guide to Durable Concrete,” Farmington Hills, MI, 84 pp., 2016.

[136] Elzbieta Horszczaruk, “Abrasion resistance of high-strength concrete in hydraulic structures,” *Wear*, vol. 259, no. 8, pp. 62–69, 2005.

[137] L. A. Sbia, A. Peyvandi, P. Soroushian, and A. M. Balachandra, “Optimization of ultra-high-performance concrete with nano- and micro-scale reinforcement,” *Cogent Eng.*, vol. 1, no. 2, pp. 1–11, 2014.

[138] Emily J. Van Dam, “Abrasion Resistance of Concrete and the Use of High Performance Concrete Railway Crossties,” *Master's thesis, Univ. Illinois Urbana-Champaign*, pp. 1–97, 2014.

[139] J. Sustersic, E. Mali, and S. Urvancic, “Erosion-Abrasion Resistance of Steel Fiber Reinforced Concrete,” *ACI Spec. Publ.,* vol. 126, pp. 729–744, 1991.

[140] ASTM C418, “Standard Test Method for Abrasion Resistance of Concrete by Sandblasting,” *West Conshohocken, PA; ASTM Int.*, pp. 10–13, 2012.

[141] ASTM C1138M, “Standard Test Method for Abrasion Resistance of Concrete (Underwater Method),” *West Conshohocken, PA; ASTM Int.*, pp. 1–5, 2019.

[142] ASTM C944, “Standard Test Method for Abrasion Resistance of Concrete or Mortar Surfaces by the Rotating-Cutter Method,” *West Conshohocken, PA; ASTM Int.*, pp. 1–5, 2019.

[143] M. Lee, Y. Wang, and C. Chiu, “A preliminary study of reactive powder concrete as a new repair material,” *Constr. Build. Mater.*, vol. 21, no. 1, pp. 182–189, 2005.

[144] B. Graybeal and J. Tanesi, “Durability of an Ultra high-Performance Concrete Durability of an Ultrahigh-Performance Concrete,” *J. Mater. Civ. Eng.*, vol. 19, no. 10, pp. 848–854,

2007.

[145] S. Pyo, S. Yihune, and H. Kim, “Abrasion resistance of ultra high performance concrete incorporating coarser aggregate,” *Constr. Build. Mater.*, vol. 165, no. 1, pp. 11–16, 2018.

[146] M. Blais, P. & Couture, “Precast , Prestressed Pedestrian Bridge- World's First Reactive Powder Concrete Structure,” *PCI Journal,* no. 5, pp. 60-71, 1999.

[147] J. Hola and K. Schabowicz, “State-of-the-art non-destructive methods for diagnostic testing of building structures – anticipated development trends,” *Arch. Civ. Mech. Eng.*, vol. 10, no. 3, pp. 5–18, 2012.

[148] D. . McCann and M. . Forde, “Review of NDT methods in the assessment of concrete and masonry structures,” *NDT E Int.*, vol. 34, no. 2, pp. 71–84, 2001.

[149] J. L. Rose, “Ultrasonic guided waves in solid media,” *Ultrason. Guid. Waves Solid Media*, pp. 1–512, Jan. 2014.

[150] Y. Dong and F. Ansari, “Non-destructive testing and evaluation (NDT/NDE) of civil structures rehabilitated using fiber reinforced polymer (FRP) composites,” in *Service Life Estimation and Extension of Civil Engineering Structures*, Woodhead Publishing, 2010, pp. 193–222.

[151] ASTM C1740, “Standard Practice for Evaluating the Condition of Concrete Plates Using the Impulse-Response Method,” *West Conshohocken, PA; ASTM Int.*, pp. 1–10, 2016.

[152] A. G. Davis, M. K. Lim, and C. G. Petersen, “Rapid and economical evaluation of concrete tunnel linings with impulse response and impulse radar non-destructive methods,” *NDT E Int.*, vol. 38, no. 3, pp. 181–186, Apr. 2005.

[153] D. Streicher, D. Algernon, J. Wöstmann, M. Behrens, and H. Wiggenhauser, “Automated NDT of port- tensioned concrete bridges using imaging echo methods,” in *9th European Conference on NDT*, 2006, pp. 1–8.

[154] ASTM C1383, “Standard Test Method for Measuring the P-Wave Speed and the Thickness of Concrete Plates Using the Impact-Echo Method,” *West Conshohocken, PA; ASTM Int.*, pp. 1–11, 2015.

[155] G. E. Stavroulakis, “Impact-echo from a unilateral interlayer crack. LCP–BEM modelling and neural identification,” *Eng. Fract. Mech.*, vol. 62, no. 2–3, pp. 165–184, Jan. 1999.

[156] J.-K. Zhang, W. Yan, D.-M. Cui, J.-K. Zhang, W. Yan, and D.-M. Cui, “Concrete Condition Assessment Using Impact-Echo Method and Extreme Learning Machines,” *Sensors*, vol. 16, no. 4, pp. 1–447, Mar. 2016.

[157] ASTM B548, “Standard Test Method for Ultrasonic Inspection of Aluminum-Alloy Plate for Pressure Vessels,” *West Conshohocken, PA; ASTM Int.*, pp. 1–5, 2017.

[158] K. Hoegh, L. Khazanovich, and H. T. Yu, "Ultrasonic Tomography for Evaluation of Concrete Pavements," *Transp. Res. Rec. J. Transp. Res. Board*, vol. 2232, no. 1, pp. 85–94, Jan. 2011.

[159] J. Martin, K. . Broughton, A. Giannopolous, M. S. . Hardy, and M. . Forde, "Ultrasonic tomography of grouted duct post-tensioned reinforced concrete bridge beams," *NDT E Int.*, vol. 34, no. 2, pp. 107–113, Mar. 2001.

[160] S. R. Doctor, T. E. Hall, and L. D. Reid, "SAFT — the evolution of a signal processing technology for ultrasonic testing," *NDT Int.*, vol. 19, no. 3, pp. 163–167, Jun. 1986.

[161] J. E. Michaels, "Detection, localization and characterization of damage in plates with an in situ array of spatially distributed ultrasonic sensors," *Smart Mater. Struct.*, vol. 17, no. 3, pp. 1–15, Jun. 2008.

[162] I. S. Lawson, I., Danso, K. A., Odoi, H. C., Adjei, C. A., Quashie, F. K., Mumuni, I. I., & Ibrahim, "Non-Destructive Evaluation of Concrete using Ultrasonic Pulse Velocity," *Res. J. Appl. Sci. Eng. Technol.*, vol. 3, no. 6, pp. 499–504, 2011.

[163] ASTM C597, "Standard Test Method for Pulse Velocity Through Concrete," *West Conshohocken, PA; ASTM Int.*, pp. 1–4, 2016.

[164] M. A. Kewalramani and R. Gupta, "Concrete compressive strength prediction using ultrasonic pulse velocity through artificial neural networks," *Autom. Constr.*, vol. 15, no. 3, pp. 374–379, May 2006.

[165] P. Wiciak, G. Cascante, and M. A. Polak, "Sensor and Dimensions Effects in Ultrasonic Pulse Velocity Measurements in Mortar Specimens," *Procedia Eng.*, vol. 193, pp. 409-416, Jan. 2017.

[166] G. Karaiskos, A. Deraemaeker, D. G. Aggelis, and D. Van Hemelrijck, "Monitoring of concrete structures using the ultrasonic pulse velocity method," *Smart Mater. Struct.*, vol. 24, no. 11, pp. 1–18, Nov. 2015.

[167] O. I. Lobkis and R. L. Weaver, "Coda-Wave Interferometry in Finite Solids: Recovery of P-to-S Conversion Rates in an Elastodynamic Billiard," *Phys. Rev. Lett.*, vol. 90, no. 25, pp. 1–4, Jun. 2003.

[168] J. Zhu and J. Popovics, "Non-contact detection of surface waves in concrete using an air-coupled sensor," *AIP Conf. Proc.*, vol. 615, no. 1, pp. 1261–1268, 2002.

[169] E. Hwang, G. Kim, G. Choe, M. Yoon, N. Gucunski, and J. Nam, "Evaluation of concrete degradation depending on heating conditions by ultrasonic pulse velocity," *Constr. Build. Mater.*, vol. 171, pp. 511–520, May 2018.

[170] F. Mielentz, "Phased Arrays for Ultrasonic Investigations in Concrete Components," *J. Nondestruct. Eval.*, vol. 27, no. 1–3, pp. 23–33, Sep. 2008.

[171] ASTM E2700, "Standard Practice for Contact Ultrasonic Testing of Welds Using Phased Arrays," *ASTM Int.*, pp. 1–9, 2014.

[172] A. V Bishko, A. A. Samokrutov, and V. G. Shevaldykin, "Ultrasonic Echo-Pulse Tomography Of Concrete Using Shear Waves Low-Frequency Phased Antenna Arrays," *Proc. 17th World Conf. Nondestruct. Test.*, vol. 25, no. 28, pp. 1–9, 2008.

[173] H. Hu *et al.*, "Stretchable ultrasonic transducer arrays for three-dimensional imaging on complex surfaces," *Sci. Adv.*, vol. 4, no. 3, pp. 1–11, Mar. 2018.

[174] A. A. Shah and Y. Ribakov, "Non-linear ultrasonic evaluation of damaged concrete based on higher order harmonic generation," *Mater. Des.*, vol. 30, no. 10, pp. 4095–4102, Dec. 2009.

[175] P. Antonaci, C. L. E. Bruno, A. S. Gliozzi, and M. Scalerandi, "Monitoring evolution of compressive damage in concrete with linear and nonlinear ultrasonic methods," *Cem. Concr. Res.*, vol. 40, no. 7, pp. 1106–1113, Jul. 2010.

[176] P. Antonaci, C. L. E. Bruno, P. G. Bocca, M. Scalerandi, and A. S. Gliozzi, "Nonlinear ultrasonic evaluation of load effects on discontinuities in concrete," *Cem. Concr. Res.*, vol. 40, no. 2, pp. 340–346, 2010.

[177] C. L. E. Bruno, A. S. Gliozzi, M. Scalerandi, and P. Antonaci, "Analysis of elastic nonlinearity using the scaling subtraction method," *Phys. Rev. B - Condens. Matter Mater. Phys.*, vol. 79, no. 6, pp. 1–13, 2009.

[178] M. Scalerandi, A. S. Gliozzi, C. L. E. Bruno, D. Masera, and P. Bocca, "A scaling method to enhance detection of a nonlinear elastic response," *Appl. Phys. Lett*, vol. 92, no. 10, p. 1-3, 2008.

[179] T. R. Hay, L. Wei, J. L. Rose, and T. Hayashi, "Rapid Inspection of Composite Skin-Honeycomb Core Structures with Ultrasonic Guided Waves," *J. Compos. Mater.*, vol. 37, no. 10, pp. 929–939, May 2003.

[180] J. L. Rose, "Ultrasonic Guided Waves in Solid Media," *Ultrason. Guid. Waves Solid Media*, pp. 1–512, 2014.

[181] H. Chan, B. Masserey, and P. Fromme, "High frequency guided ultrasonic waves for hidden fatigue crack growth monitoring in multi-layer model aerospace structures," *Smart Mater. Struct.*, vol. 24, no. 2, pp. 1–10, 2015.

[182] M. Hirao, H. Ogi, and H. Fukuoka, "Resonance EMAT system for acoustoelastic stress measurement in sheet metals," *Rev. Sci. Instrum.*, vol. 64, no. 11, pp. 3198–3205, 1993.

[183] P. Wilcox, M. Lowe, and P. Cawley, "Omnidirectional guided wave inspection of large metallic plate structures using an EMAT array," *IEEE Trans. Ultrason. Ferroelectr. Freq. Control*, vol. 52, no. 4, pp. 653–665, 2005.

[184] S. Guide, “Standard Guide for Electromagnetic Acoustic Transducers (EMATs),” *Significance*, vol. 3, pp. 1–8, 2002.

[185] C. B. Thring, Y. Fan, and R. S. Edwards, “Multiple focused EMAT designs for improved surface breaking defect characterization,” *AIP Conf. Proc.*, vol. 1806, no. 1, 2017.

[186] ASTM E1962, “Standard Practice for Ultrasonic Examinations Using Electromagnetic Acoustic Transducer (EMAT) Techniques,” *West Conshohocken, PA; ASTM Int.*, pp. 1–10, 2019.

[187] J. Maser *et al.*, “Soft X-ray microscopy with a cryo scanning transmission X-ray microscope: I. Instrumentation, imaging and spectroscopy,” *J. Microsc.*, vol. 197, no. 1, pp. 68–79, 2000.

[188] A. Rundquist *et al.*, “Phase-matched generation of coherent soft X-rays,” *Science*, vol. 280, no. 5, pp. 1412–1415, May 1998.

[189] Z. Chang, A. Rundquist, H. Wang, M. M. Murnane, and H. C. Kapteyn, “Generation of Coherent Soft X Rays at 2.7 nm Using High Harmonics,” *Phys. Rev. Lett.*, vol. 79, no. 16, pp. 2967–2970, 1997.

[190] J. M. Rodenburg *et al.*, “Hard-X-Ray Lensless Imaging of Extended Objects,” *Phys. Rev. Lett.*, vol. 98, no. 3, pp. 1–4, 2007.

[191] E. J. Hall and D. J. Brenner, “Cancer risks from diagnostic radiology,” *Br. J. Radiol.*, vol. 81, no. 2, pp. 362–378, May 2008.

[192] R. D. Owen, “Portable linear accelerators for X-ray and electron-beam applications in civil engineering,” *NDT E Int.*, vol. 31, no. 6, pp. 401–409, Dec. 1998.

[193] L. Peng, J. Bai, X. Zeng, and Y. Zhou, “Comparison of isotropic and orthotropic material property assignments on femoral finite element models under two loading conditions,” *Med. Eng. Phys.*, vol. 28, no. 3, pp. 227–233, Apr. 2006.

[194] T. S. Oesch, E. N. Landis, and D. A. Kuchma, “Conventional Concrete and UHPC Performance–Damage Relationships Identified Using Computed Tomography,” *J. Eng. Mech.*, vol. 142, no. 12, pp. 1–10, Dec. 2016.

[195] T. Ruan and A. Poursaee, “Fiber-Distribution Assessment in Steel Fiber–Reinforced UHPC Using Conventional Imaging, X-Ray CT Scan, and Concrete Electrical Conductivity,” *J. Mater. Civ. Eng.*, vol. 31, no. 8, pp. 1–7, Aug. 2019.

[196] T. Oesch, E. Landis, and D. Kuchma, “A methodology for quantifying the impact of casting procedure on anisotropy in fiber-reinforced concrete using X-ray CT,” *Mater. Struct. Constr.*, vol. 51, no. 3, pp. 1–13, 2018.

[197] H. Saleh and R. Livingston, “Experimental Evaluation of a Portable Neutron-Based Gamma-Spectroscopy System for Chloride Measurements in Reinforced Concrete,” *J.*

Radioanal. Nucl. Chem., vol. 244, no. 2, pp. 367–371, May 2000.

[198] K. Karhunen, A. Seppänen, A. Lehikoinen, P. J. M. Monteiro, and J. P. Kaipio, "Electrical Resistance Tomography imaging of concrete," *Cem. Concr. Res.*, vol. 40, no. 1, pp. 137–145, Jan. 2010.

[199] F. Wenner, "A method for measuring Earth resistivity," *Source J. Washingt. Acad. Sci.*, vol. 5, no. 16, pp. 561–563, 1915.

[200] B. Shafei, B. Phares, M. Najimi, and T. Hosteng, "Laboratory and Field Evaluation of an Alternative UHPC Mix and Associated UHPC Bridge," *Bridg. Eng. Center, iowa Highw. Res. Board*, vol. 515, pp. 1–80, 2019.

[201] B. Elsener, C. Andrade, J. Gulikers, R. Polder, and M. Raupach, "Half-cell potential measurements—Potential mapping on reinforced concrete structures," *Mater. Struct.*, vol. 36, no. 7, pp. 461–471, 2003.

[202] ASTM C876, "ASTM C 876 Standard Test Method for Corrosion Potentials of Uncoated Reinforcing Steel in Concrete," *West Conshohocken, PA; ASTM Int.*, pp. 1–8, 2016.

[203] M. F. Md Jaafar, H. Mohd Saman, N. F. Ariffin, K. Muthusamy, S. Wan Ahmad, and N. Ismail, "Corrosion monitoring on steel reinforced nano metaclayed-UHPC towards strain modulation using fiber Bragg grating sensor," *IOP Conf. Ser. Mater. Sci. Eng.*, vol. 431, no. 12, pp. 1–8, Nov. 2018.

[204] H. Elsener, B., Klinghoffer, O., Frolund, T., Rislund, E., Schiegg, Y., & Böhni, "Assessment of reinforcement corrosion by means of galvanostatic pulse technique," *Procedings Int. Conf. Repair Concr. Struct. Theory to Pract. a Mar. Environ.*, pp. 391–400, 1997.

[205] ASTM C876, "Standard test method for half-cell potentials ofuncoated reinforcing steel in concrete," *West Conshohocken, PA; ASTM Int.*, p. 1-8, 2015.

[206] J. M. Torrents, A. Blanco, P. Pujadas, A. Aguado, P. Juan-García, and M. Á. Sánchez-Moragues, "Inductive method for assessing the amount and orientation of steel fibers in concrete," *Mater. Struct. Constr.*, vol. 45, no. 10, pp. 1577–1592, 2012.

[207] H. Kim, D. Kang, S. J. Oh, and C. Joo, "Nondestructive evaluation on dispersion of steel fibers in UHPC using THz electromagnetic waves," *Constr. Build. Mater.*, vol. 172, no. 5, pp. 293–299, 2018.

[208] A. Robert, "Dielectric permittivity of concrete between 50 Mhz and 1 Ghz and GPR measurements for building materials evaluation," *J. Appl. Geophys.*, vol. 40, no. 1–3, pp. 89–94, Oct. 1998.

[209] C. Maierhofer, "Nondestructive evaluation of concrete infrastructure with ground penetrating radar," *J. Mater. Civ. Eng.*, vol. 15, no. 3, pp. 287–297, 2003.

[210] L. D. Favro, R. L. Thomas, X. Han, Z. Ouyang, G. Newaz, and D. Gentile, "Sonic infrared imaging of fatigue cracks," *Int. J. Fatigue*, vol. 23, no. 1, pp. 471–476, 2001.